

1 Labilization and diversification of pyrogenic dissolved organic matter by 2 microbes

3
4 Aleksandar I. Goranov^{1,*}, Andrew S. Wozniak², Kyle W. Bostick^{3,†}, Andrew R. Zimmerman³, Siddhartha
5 Mitra⁴, and Patrick G. Hatcher¹

6
7 ¹Department of Chemistry and Biochemistry, Old Dominion University, Norfolk, VA, USA

8 ²School of Marine Science and Policy, College of Earth, Ocean, and Environment, University of Delaware, Lewes, DE, USA

9 ³Department of Geological Sciences, University of Florida, Gainesville, FL, USA

10 ⁴Department of Geological Sciences, East Carolina University, Greenville, NC, USA

11
12 *Correspondence to:* Patrick G. Hatcher (phatcher@odu.edu)

13 14 **Abstract**

15
16 With the increased occurrence of wildfires around the world, interest in the chemistry of pyrogenic organic
17 matter (pyOM) and its fate in the environment has increased. Upon leaching from soils by rain events, significant
18 amounts of dissolved pyOM (pyDOM) enter the aquatic environment and interact with microbial communities
19 that are essential for cycling organic matter within the different biogeochemical cycles. To evaluate the bio-
20 degradability of pyDOM, aqueous extracts of laboratory-produced biochars were incubated with soil microbes
21 and the molecular changes to the composition of pyDOM were probed using ultrahigh resolution mass
22 spectrometry (Fourier transform – ion cyclotron resonance – mass spectrometry). Given that solar irradiation
23 significantly affects the composition of pyDOM during terrestrial-to-marine export, the effects of photochemistry
24 were also evaluated in the context of pyDOM bio-degradability.

25 Ultrahigh resolution mass spectrometry revealed that many different (both aromatic and aliphatic)
26 compounds were bio-degraded. New labile compounds, 22 – 40 % of which were peptide-like, were bio-produced.
27 These results indicated that a portion of pyDOM has been labilized into microbial biomass during the incubations.
28 Fluorescence excitation-emission matrix spectra revealed that some fraction of these new bio-produced molecules
29 is associated with proteinaceous fluorophores. Two-dimensional ¹H-¹H total correlation NMR spectroscopy
30 identified a peptidoglycan-like backbone within the microbially produced compounds. These results are
31 consistent with previous observations of peptidoglycans within the soil and ocean nitrogen cycles where remnants
32 of bio-degraded pyDOM are expected to be observed.

33 Interestingly, the exact nature of the bio-produced organic matter was found to vary drastically among
34 samples indicating that the used microbial consortium may produce different exudates based on the composition
35 of the initial pyDOM. Another potential explanation for the vast diversity of molecules is that microbes only
36 consume low molecular weight compounds, but they also produce reactive oxygen species (ROS), which initiate
37 oxidative and recombination reactions that produce new molecules. Some of the bio-produced molecules (212 –
38 308 molecular formulas) were identified in surface and abyssal oceanic samples and 81 – 192 of them were of
39 molecular composition attributed to carboxyl-rich alicyclic molecules (CRAM). These results indicate that some
40 of the pyDOM bio-degradation products have an oceanic fate and can be sequestered into the deep ocean. The
41 observed microbially-mediated diversification of pyDOM suggests that pyDOM contributes to the observed large
42 complexity of natural organic matter observed in riverine and oceanic systems. More broadly, our research shows
43 that pyDOM can be substrate for microbial growth and be incorporated into environmental food webs within the
44 global carbon and nitrogen cycles.

45

* Current Address: Department of Earth and Environmental Sciences, Rensselaer Polytechnic Institute, Troy, NY, USA

† Current Address: Fugro GeoServices, 6100 Hillcroft Avenue, Houston, TX, USA

1 Introduction

Pyrogenic organic matter (pyOM), the carbonaceous solid residue that is left after biomass burning (e.g., wildfires, biochar production), has been gaining attention in recent years as an important active component of the global biogeochemical cycles. Compositionally, pyOM is mainly comprised of condensed aromatic compounds (ConAC) of various degrees of condensation and functionalization (Masiello, 2004; Schneider et al., 2010; Wagner et al., 2018; Wozniak et al., 2020). ConAC have been found in various environmental matrices such as soils and sediments (Schmidt and Noack, 2000; Skjemstad et al., 2002; Reisser et al., 2016) and atmospheric aerosols (Wozniak et al., 2008; Bao et al., 2017). In the terrestrial environmental matrices, particularly in soils and sediments, ConAC were originally thought to be highly stable (“recalcitrant”) due to their condensed character (Goldberg, 1985; Masiello and Druffel, 1998). However, more and more studies report of the presence of pyrogenic molecules in different aquatic environments (Hockaday et al., 2006; Dittmar and Paeng, 2009; Roebuck et al., 2017; Wagner et al., 2017; Li et al., 2019). These studies support the proposition that pyOM can be solubilized upon rain events and be leached as pyrogenic dissolved organic matter (pyDOM) resulting in large annual riverine fluxes of pyDOM from global riverine systems to the open ocean (Dittmar et al., 2012; Jaffé et al., 2013; Wang et al., 2016; Marques et al., 2017; Jones et al., 2020). During export, pyDOM is likely altered by various processes resulting in its degradation and alteration of its physico-chemical characteristics (Masiello, 2004; Coppola et al., 2019; Wagner et al., 2019). Using laboratory-prepared biochars and conservative assumptions, Bostick et al. (2018) approximated that > 85% of the leached pyDOM is degradable (e.g., mineralizable to CO₂), which indicates that pyDOM is a very active component within the global carbon cycle, as previously suggested (Druffel, 2004; Lehmann, 2007; Riedel et al., 2016).

In sunlit aquatic environments, photo-degradation is the most significant sink for the ConAC fraction of pyDOM (Stubbins et al., 2012). The photochemistry of ConAC and pyDOM has been studied utilizing either laboratory-prepared pyDOM (Ward et al., 2014; Fu et al., 2016; Li et al., 2019; Bostick et al., 2020; Goranov et al., 2020; Wang et al., 2020) or ConAC-rich natural organic matter (Stubbins et al., 2010, 2012; Wagner and Jaffé, 2015). These studies have reported that ConAC are exceptionally photo-labile and they degrade through a series of oxygenation, ring-opening, and decarboxylation reactions leading to a pool of smaller aliphatic by-products. Additionally, pyDOM photochemistry has been associated with the production of high fluxes of reactive oxygen species (ROS), important transients involved in the photo-transformation and photo-degradation of pyDOM (Fu et al., 2016; Li et al., 2019; Goranov et al., 2020; Wang et al., 2020). These studies have contributed to a better understanding of the biogeochemical cycling of pyDOM in the presence of sunlight in the environment. Microbial (biotic) pathways are another degradative pathway with high potential for altering and/or mineralizing pyDOM, but these pathways are far less understood.

Biotic reworking of organic molecules is a key mechanism for producing the diverse molecular composition of natural organic matter (Lechtenfeld et al., 2015; Hach et al., 2020). Due to the highly condensed character of pyOM, it is often regarded as bio-recalcitrant, though several studies have shown that a fraction of it (about 0.5 to 10 %) is indeed bio-degradable (Kuzyakov et al., 2009, 2014; Zimmerman, 2010; Zimmerman et al., 2011). PyOM is mainly comprised of ConAC (Bostick et al., 2018; Wozniak et al., 2020), which contributes to its low bio-degradability (Zimmerman, 2010). By contrast, pyDOM is highly heterogeneous (Wozniak et al., 2020), and in addition to ConAC, it contains numerous low molecular weight (LMW) species (e.g., acetate, methanol, formate; Bostick et al., 2018; Goranov et al., 2020) as well as various pyrogenic aliphatic compounds and inorganic nutrients (Hockaday et al., 2007; Mukherjee and Zimmerman, 2013; Goranov et al., 2020; Wozniak et al., 2020). The high solubility of pyDOM is imparted by the greater abundance of polar functional groups, which would also allow for greater microbial accessibility. To date, there is no study that evaluates the molecular-scale bio-degradability of pyDOM. It is unknown whether and how (e.g., mechanistic pathways, kinetic rates) the different compound groups of pyDOM are bio-degraded and/or bio-transformed.

In addition to the unexplored bio-degradability of pyDOM, there are concerns that biochar leachates may be toxic due to the presence of condensed and ligninaceous aromatics. It has been shown that cellulose- and pinewood-derived biochar water-extracts (i.e., pyDOM) inhibit the growth of cyanobacteria while pyDOM of lignin-derived biochar has no inhibitory effects (Smith et al., 2016). The toxicity of pyDOM has been mainly

96 attributed to polysubstituted phenols present in the cellulose- and pinewood-derived biochars. In natural systems,
97 however, it is likely that other pyDOM components also play a role in controlling the bio-degradability and
98 toxicity of pyDOM. An important very recent finding is that pyOM and pyDOM contain organochlorine
99 compounds (both aliphatic and aromatic; Wozniak et al., 2020), which may enhance the toxicity of pyDOM.
100 Thus, biotic incubations of pyDOM are needed to reveal if microbial growth can be sustained in pyDOM/ConAC-
101 rich environments.

102 To explore these questions, we incubated aqueous biochar leachates (i.e., pyDOM) with a soil-derived
103 microbial consortium and evaluated the compositional changes to pyDOM using numerous analytical techniques.
104 Laboratory-produced biochars can be considered model pyrogenic substances as they are similar to what is
105 produced during natural wildfires (Santín et al., 2017) but have not experienced environmental aging which would
106 have impacted their physico-chemical properties (Ascough et al., 2011). We have used oak wood because most
107 of riverine dissolved organic matter (DOM) is exported from forested catchments (Hedges et al., 1997). We used
108 two pyrolysis temperatures (400 and 650 °C) representative of forest fire temperatures (Santín et al., 2015, 2016).
109 As photochemistry has been shown to increase the bio-lability of various types of DOM (Kieber et al., 1989;
110 Lindell et al., 1995; Wetzel et al., 1995; Benner and Biddanda, 1998; Moran and Covert, 2003; Qualls and
111 Richardson, 2003; Obernosterer and Benner, 2004; Abboudi et al., 2008; Chen and Jaffé, 2014; Antony et al.,
112 2018), we also incubated pyDOM that had been photo-irradiated. Previous studies showed that significant
113 compositional changes occur to pyDOM during photo-irradiation, which certainly implies different bio-
114 degradability (Bostick et al., 2020; Goranov et al., 2020).

115 In a parallel study of the same incubations (Bostick et al., 2021), we quantified the total organic carbon
116 (TOC) loss, respired CO₂ quantities, as well as the changes to the bulk structural composition of pyDOM as
117 determined by one-dimensional ¹H nuclear magnetic resonance (NMR) spectroscopy. Additionally, in that study,
118 benzenepolycarboxylic acid (BPCA) molecular markers were used to quantify the changes specific to the ConAC
119 fraction of pyDOM. It was found that the pyDOM leachates derived from the biochar of higher pyrolysis
120 temperature (650 °C) were less bio-degradable than the pyDOM leachates from the lower temperature (400 °C)
121 biochar. As expected, photo-irradiation increased the bio-lability of pyDOM. Over the 96-day incubation, up to
122 48% of the carbon was respired to CO₂. The degradation followed first-order kinetics, with LMW compounds
123 (e.g., acetate, formate, methanol) being preferentially degraded. To elucidate the molecular-level changes taking
124 place during the bio-incubation of pyDOM, and assess the various molecules that are being degraded or produced
125 by soil biota, we employed ultrahigh resolution mass spectrometry (Fourier transform – ion cyclotron resonance
126 – mass spectrometry, FT-ICR-MS), two-dimensional NMR, and fluorescence spectroscopy. The collective results
127 from these two studies improve our understanding of the degradative pathways of pyDOM and ConAC in the
128 environment and allow us to better interpret observations pertaining to terrestrial-to-marine transfers and global
129 cycling of organic matter.

131 2 Materials and Methods

133 2.1 Preparation of pyDOM samples

135 Two biochars were prepared by heating laurel oak wood (*Quercus hemisphaerica*) under N₂ atmosphere
136 at 400 and 650 °C for 3 hours. After grinding and sieving to particles of uniform size (0.25 - 2.00 mm), the
137 biochars were leached in 18.1 mΩ MilliQ laboratory-grade water (5 g in 500 mL) over 50 hours on a shaker table.
138 The obtained pyDOM leachates, hereafter referred to as “Oak 400 Fresh” and “Oak 650 Fresh”, were filtered
139 using 0.2 μm Millipore GSWP mixed cellulose ester filters. Physico-chemical characteristics of similarly
140 produced solid biochars and their leachates were reported in several previous studies (Zimmerman, 2010;
141 Mukherjee et al., 2011; Bostick et al., 2018; Wozniak et al., 2020). A fraction of each leachate was also subjected
142 to photo-irradiation for 5 days in a custom-made solar simulator equipped with Q-Lab Corporation UV-A lamps
143 (295 – 365 nm, λ_{MAX} = 340 nm, 40 watt) equivalent to natural photo-irradiation of 12 days. Photo-transformation
144 rates, structural changes, photo-irradiation apparatus design, and other relevant information have been published
145 previously (Bostick et al., 2020; Goranov et al., 2020). Photo-irradiated pyDOM samples will be hereafter referred

146 to as “Oak 400 Photo” and “Oak 650 Photo”. The four samples (Oak 400 Fresh, Oak 650 Fresh, Oak 400 Photo,
147 Oak 650 Photo) were diluted to a uniform TOC concentration of $4.7 \text{ mgC}\cdot\text{L}^{-1}$ prior to inoculation.
148

149 **2.2 Microbial incubations of pyDOM**

150

151 Microbial incubations were performed using a soil-derived microbial consortium as an inoculum. Soil
152 from the Austin Cary Memorial Forest (Gainesville, FL) was chosen, because this area is frequently subjected to
153 prescribed burns (Johns, 2016), and its soil microbes likely interact with pyOM and pyDOM on a regular basis.
154 Taxonomic details of the used soil have been published previously (Khodadad et al., 2011). The collected soil
155 was treated to remove roots and detritus, and its water-extract was centrifuged to obtain a pellet. The pellet was
156 then dissolved in 10 mL MilliQ laboratory-grade water to obtain an inoculate, 100 μL of which was used to spike
157 50 mL of each pyDOM substrate. Additionally, microbial nutrients (KH_2PO_4 and $(\text{NH}_4)_2\text{SO}_4$) were provided
158 following Zimmerman (2010) to support a healthy growth medium. Samples were incubated in gas-sealed amber
159 vials on a shaker table at $28 \pm 5 \text{ }^\circ\text{C}$ for 10 days in the dark. Using a double-needle assembly, CO_2 -free air (Airgas,
160 Zero) was flushed through the samples on days 0, 2, 5, and 10, which oxygenated the samples and removed
161 dissolved inorganic carbon for its measurement (reported by Bostick et al. (2021)). A procedural blank and control
162 samples were prepared in the exact same way but were poisoned with HgCl_2 immediately following the mixing
163 of the different components (pyDOM, inoculate, nutrients). Additionally, a solution of sucrose ($0.5 \text{ g C}_{12}\text{H}_{22}\text{O}_{11}$
164 in 40 mL MilliQ laboratory-grade water) was also incubated in the same manner to serve as a positive control.
165 All incubated samples were poisoned with HgCl_2 to terminate microbial activity before shipment to Old Dominion
166 University (Norfolk, VA) for analysis. Prior to spectroscopic analysis (see Sect. 2.3 and 2.5 below) or
167 spectrometric analysis (see Sect. 2.4 below), samples were filtered using acid-washed $0.1 \text{ }\mu\text{m}$ Teflon (PTFE)
168 syringe filters. Further details about sample preparation can be found in the parallel study (Bostick et al., 2021).
169

170 **2.3 Analysis of chromophoric and fluorophoric dissolved organic matter**

171

172 Chromophoric DOM (CDOM) measurements were performed on a Thermo Scientific Evolution 201
173 ultraviolet-visible (UV-VIS) spectrophotometer operated in a double-beam mode. A matched Starna quartz
174 cuvette with MilliQ water was used as a reference during all spectral measurements. Spectra were recorded from
175 230 – 800 nm using a 1 nm step, 0.12 s integration time, and 500 nm/min scan speed. In addition to the double-
176 beam referencing, the average noise in the 700-800 nm spectral region was subtracted from the spectra to correct
177 for any instrument baseline drifts, temperature fluctuations, as well as scattering and refractive effects (Green and
178 Blough, 1994; Helms et al., 2008). After consecutive procedural-blank corrections, the spectra (kept in decadic
179 units) were normalized to the cuvette path length (1.0 cm) and TOC content (in $\text{mgC}\cdot\text{L}^{-1}$) to convert them to
180 specific absorbance spectra ($\text{L}\cdot\text{mgC}^{-1}\cdot\text{cm}^{-1}$; Weishaar et al., 2003). CDOM was quantified by integrating the
181 spectra from 250 – 450 nm (Helms et al., 2008) and CDOM quantity is reported in $\text{L}\cdot\text{mgC}^{-1}\cdot\text{cm}^{-1}\cdot\text{nm}$ units.

182 Fluorophoric DOM (FDOM) measurements were performed on a Shimadzu RF-6000 spectrofluorometer
183 operated in 3D acquisition mode. Samples were analyzed without dilution as no sample yielded absorbance at
184 230 nm above 0.07 (Miller et al., 2010). Samples were excited from 230 – 500 nm (5 nm step) and emission was
185 recorded over 250 – 650 nm (5 nm step) to obtain excitation-emission matrices (EEMs). Additionally, five
186 replicate water Raman scans were acquired on MilliQ water in 2D emission mode by exciting the sample at 350
187 nm and fluorescence intensity was monitored over 365 – 450 nm (0.5 nm steps). All measurements were done
188 with 5 nm slit widths of the monochromators, 600 nm/min scan speed, and in high-sensitivity mode.

189 EEMs were processed in MATLAB using the drEEM toolbox (version 0.4.0.) using previously published
190 routines (Murphy et al., 2010, 2013). Briefly, using the *FDOMcorrect* function, the raw EEMs were adjusted for
191 instrumental bias, blank-corrected using an EEM of the procedural blank, and scaled to adjust for any inner-filter
192 effects using the raw UV-VIS spectra (Kothawala et al., 2013). This function also normalized the EEMs to Raman
193 units (RU) after the area of the water Raman peak (peak maximum at 397 nm) had been determined by the
194 *ramanintegrationrange* function (Murphy, 2011) on the averaged water Raman spectrum. The EEMs were then

195 processed using the *smootheem* function to remove 1st and 2nd order Rayleigh signals and Raman scattering. EEMs
196 are visualized and difference plots are generated using an in-house MATLAB script.

197 198 **2.4 Fourier transform - ion cyclotron resonance - mass spectrometry (FT-ICR-MS)** 199

200 Procedural blank, control, and incubated samples were loaded onto solid-phase extraction cartridges
201 (Agilent Technologies Bond Elut PPL, 100 mg styrene divinyl copolymer) as previously described (Dittmar et
202 al., 2008). Cartridges were eluted with methanol (Fisher Scientific, Optima LC-MS grade) and infused into an
203 Apollo II electrospray ionization (ESI) source interfaced with a Bruker Daltonics Apex Qe FT-ICR-MS operating
204 at 10 T and housed in the College of Sciences Major Instrumentation Cluster (COSMIC) facility at Old Dominion
205 University (Norfolk, VA). The instrument is externally calibrated daily with a polyethylene glycol standard and
206 a surrogate laboratory pyDOM standard was analyzed before and after the analytical sequence to verify for the
207 lack of instrumental drift. Additionally, an instrumental blank of methanol was analyzed between samples to
208 verify for the absence of sample carryover. Samples were analyzed in negative ionization mode. ESI spray
209 voltages were optimized for each sample to assure for consistent spray currents among all samples. For each
210 sample, 300 transients with a 4MWord time domain were collected, co-added, and the resultant free induction
211 decay was zero-filled and sine-bell apodized. After fast Fourier transformation, internal calibration of the resultant
212 mass spectra was performed using naturally abundant fatty acids, dicarboxylic acids, and compounds belonging
213 to the CH₂-homologous series as previously described (Sleighter et al., 2008). Then, using an in-house MATLAB
214 script, salt, blank, and isotopologue (¹³C, ³⁷Cl) peaks were removed. Molecular formulas within ± 1 ppm error
215 were assigned to FT-ICR-MS spectral peaks (S/N ≥ 3) using the Molecular Formula Calculator from the National
216 High Magnetic Field Laboratory (Tallahassee, FL). Formula assignments were restricted to elemental
217 composition of ¹²C_{5-∞}, ¹H_{1-∞}, ¹⁴N₀₋₅, ¹⁶O₀₋₃₀, ³²S₀₋₂, ³¹P₀₋₂, and ³⁵Cl₀₋₄, and were refined using previously established
218 rules (Stubbins et al., 2010). Any ambiguous peak assignments were refined by inclusion within homologous
219 series (CH₂, H₂, COO, CH₂O, O₂, H₂O, NH₃, HCl) following Kujawinski and Behn (2006) and Koch et al. (2007).
220 For all samples, at least 80% of the mass spectral peaks were assigned, and they accounted for at least 93% of the
221 mass spectral magnitude.

222 Molecular composition was evaluated by plotting the molecular formulas on van Krevelen (vK) diagrams,
223 scatterplots of the formulas' hydrogen-to-carbon (H/C) versus oxygen-to-carbon (O/C) ratios (Van Krevelen,
224 1950; Kim et al., 2003). Formulas were further categorized using the modified aromaticity index (AI_{MOD}), a proxy
225 for the aromatic character of molecules (Koch and Dittmar, 2006, 2016), and calculated as shown in Eq.1.

$$226 \quad AI_{MOD} = \frac{1 + C - \frac{1}{2}O - S - \frac{1}{2}(N + P + H + Cl)}{C - \frac{1}{2}O - N - S - P} \quad \text{Eq. 1}$$

227 Formulas were classified as following: Condensed aromatic compounds (ConAC, AI_{MOD} ≥ 0.67, number
228 of C-atoms ≥ 15), aromatic (0.67 < AI_{MOD} ≤ 0.50), olefinic/alicyclic (0 < AI_{MOD} < 0.50), and aliphatic (AI_{MOD} =
229 0). Additionally, N-containing formulas falling in the ranges of 1.5 ≤ H/C ≤ 2 and 0.1 ≤ O/C ≤ 0.67 were classified
230 as peptide-like. Statistical evaluation of means using one-way analysis of variance (ANOVA) was performed in
231 MATLAB using the *anova1* function. Post-hoc Scheffé's assessments were performed using the *multcompare*
232 function. Pearson correlations were performed using the *corrcoef* function in the same software. Confidence level
233 of 95% was used for all statistical assessments.

234 For the Kendrick mass defect (KMD) series analysis (described later in the manuscript), Kendrick mass
235 (KM) was first calculated using the molecular weight of each compound (i.e., calculated mass from its molecular
236 formula) following Eq. 2. Then, the Kendrick nominal mass (KNM) was calculated as the integer (no decimals)
237 of the Kendrick mass (KM) as shown in Eq. 3. The Kendrick nominal mass (KMD) is the difference between KM
238 and KNM, i.e., the decimals (Eq. 4). This analysis was performed for oxygen (O), carbonyl (CO), and carboxyl
239 (COO) series (S).
240

$$\text{KM} = \text{Molecular Weight} \times \text{S} \quad \text{Eq. 2}$$

$$\text{where } S = \frac{16.0000000}{15.9949146} \text{ for O series; } \frac{28.0000000}{27.9949146} \text{ for CO series; and } \frac{44.0000000}{43.9898292} \text{ for COO series}$$

$$\text{KNM} = \text{integer of KM} \quad \text{Eq. 3}$$

$$\text{KMD} = \text{KM} - \text{KNM} \quad \text{Eq. 4}$$

242

243

244

2.5 Two-dimensional nuclear magnetic resonance (NMR) spectroscopy

245

246

247

248

249

250

251

252

253

254

255

256

257

258

259

260

261

262

263

264

265

266

267

268

269

270

271

272

273

274

275

276

277

278

279

280

281

282

283

One-dimensional ^1H NMR spectra of the samples were published and evaluated in the parallel study (Bostick et al., 2021). For the study of this manuscript, a select sample was analyzed using two-dimensional ^1H - ^1H total correlation spectroscopy (TOCSY) to further evaluate several functional groups of interest. Analyses were performed on a 400 MHz (9.4 Tesla) Bruker BioSpin AVANCE III spectrometer fitted with a double-resonance broadband z-gradient inverse (BBI) probe in the COSMIC facility. Samples were analyzed without pre-concentration and volumetrically diluted with deuterated water (D_2O , Acros Organics, 100% D) to obtain a 90:10 $\text{H}_2\text{O}:\text{D}_2\text{O}$ solution. Further details of sample preparation and acquisition of 1D ^1H spectra are published in the companion study (Bostick et al., 2021). To obtain ultraclean NMR spectra, NMR tubes were soaked with aqua regia, rinsed extensively with ultrapure water, and individually tested as blanks to verify that no background peaks are present. While ^1H spectra were originally processed using an exponential multiplication function (line broadening) of 5 Hz to obtain higher signal-to-noise for a more accurate and precise integration (Bostick et al., 2021), here they were re-processed using a multiplication function of 1.5 Hz to better observe the splitting (multiplicity) patterns of the peaks of interest. TOCSY spectra were acquired using the phase-sensitive gradient-enhanced mlevgpphw5 pulse program. It utilizes a 17-step Malcolm Levitt (MLEV-17) composite scheme (Bax and Davis, 1985) for magnetization transfer between any coupled nuclear spins, and a W5-WATERGATE element for water suppression (Liu et al., 1998). Both short-range and long-range spin-spin couplings were observed using 30 ms and 100 ms mixing times, respectively. The data were then zero-filled to a 4096 x 1024 matrix and then fitted with a $\pi/2$ -shifted (SSB = 2) sine-squared window function. Linear prediction to 256 points was used in the F_1 dimension. All spectra were internally calibrated to the sharp distinguishable methanol singlet at 3.34 ppm (Gottlieb et al., 1997), and then spectra were phased and baseline-corrected. T_1 -noise removal was performed by calculating the positive projection of rows with no resonances and the summed projections were subtracted from all rows in the spectrum (Klevit, 1985). The same procedure was performed for all columns (F_2 dimension).

3 Results

3.1 Molecular changes to pyDOM after microbial incubation

Ultrahigh resolution mass spectrometric analysis of the bio-incubated and corresponding control pyDOM leachates revealed significant changes in molecular composition after the 10-day incubation (Fig. 1). The identified molecular formulas were classified into one of three groups using a presence-absence approach (Stubbins et al., 2010; Sleighter et al., 2012). This approach identifies any common formulas among the two samples being compared (control and bio-incubated), as well as any formulas that are unique to each sample. It is important to note that the electrospray ionization (ESI) source is prone to biases, and the analytical window of FT-ICR-MS depends most critically on it. Thus, it may not identify compounds that are present if they are not ionizable (Stenson et al., 2002; Patriarca et al., 2020). Therefore, our observations are influenced by the limited analytical window, and it is essential that observations by FT-ICR-MS are always paired with supplementary quantitative techniques (optical analyses, NMR, etc.) in order to determine if the identified trends are real or an artifact of ESI charge competition (D'Andrilli et al., 2020).

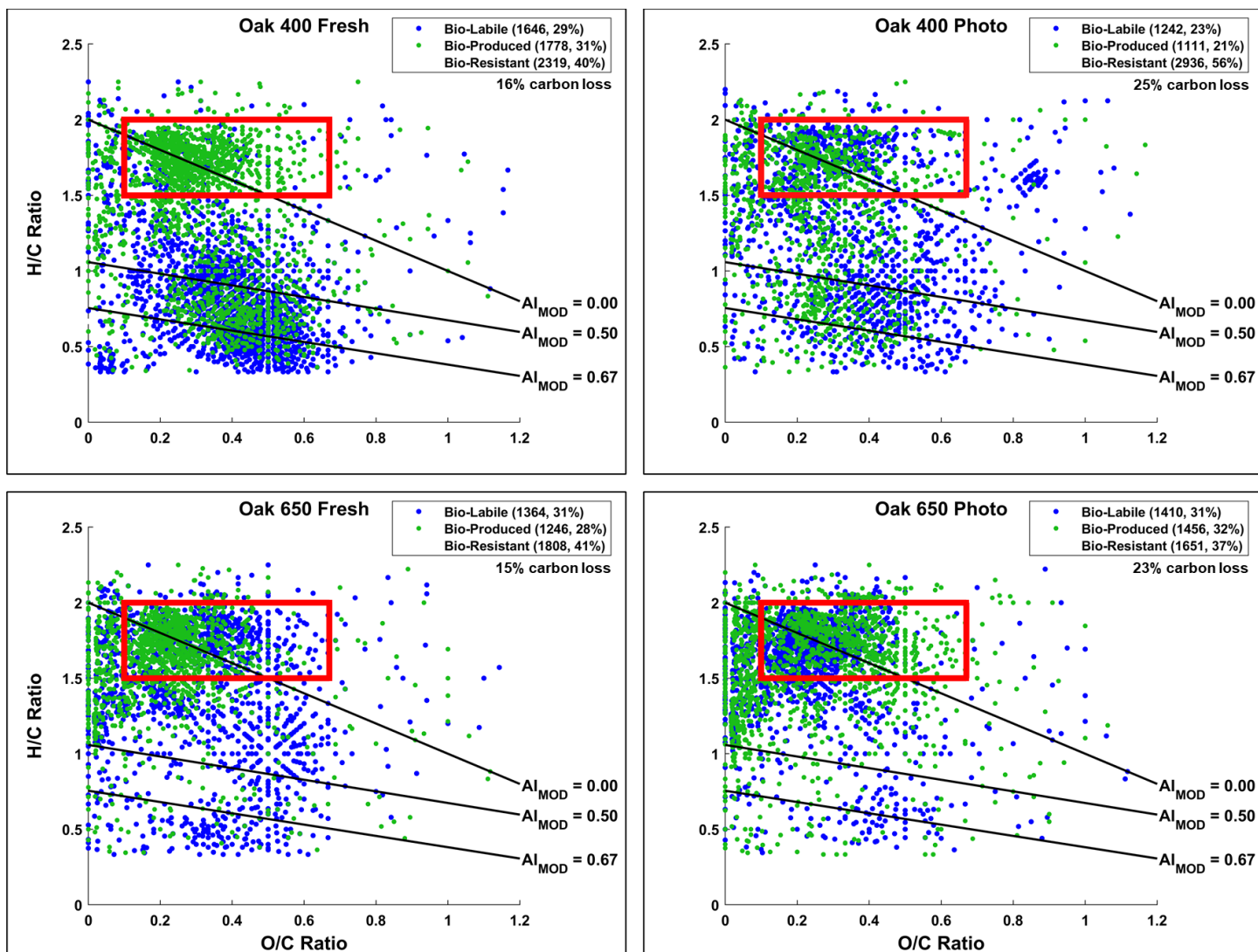


Figure 1. Van Krevelen (vK) diagrams of 10-day microbially incubated pyDOM leachates. Formulas are classified as **bio-labile** (formulas only found in the “killed” control pyDOM leachates) and **bio-produced** (formulas only found in the bio-incubated samples). Formulas that are present in both the control and bio-incubated samples are operationally classified as bio-resistant and not shown for clarity. These three classes of molecules are separately plotted on vK diagrams and shown in Sect. 2 of the Supplement (Figs. S2-4). The number of formulas found in each of these pools is listed in the legends along with corresponding percentages (relative to total number of formulas in the two samples being compared). The carbon losses quantified by Bostick et al. (2021) are listed under the legends. The **black** lines indicate modified aromaticity index cutoffs (AI_{MOD}; Koch and Dittmar, 2006, 2016), and the **red** box indicates the peptide region (valid only for N-containing formulas).

In all samples, nearly a third of the formulas (23 – 31%) present in the control samples were not observed after the biotic incubations. This is somewhat proportional to the organic carbon losses observed over the 10-day incubation by Bostick et al. (2021). The organic carbon loss was also found to be equivalent to mineralized CO₂ ($\pm 4\%$, Bostick et al., 2021) indicating that microbial respiration had occurred though CO₂ mineralization can happen abiotically as well. Using the number of formulas lost as a proxy for bio-lability here, it appears that Oak 400 Fresh (1646 bio-labile formulas, 16% carbon loss) is more bio-labile than Oak 650 Fresh (1364 bio-labile formulas, 15% carbon loss). This was expected because of the richness of Oak 400 Fresh in smaller less-aromatic compounds (Wozniak et al., 2020). Upon photo-irradiation, both Oak 400 Fresh and Oak 650 Fresh experience significant changes in their molecular composition as previously described in detail by Goranov et al. (2020). The photo-transformed pyDOM is much more aliphatic and richer in nitrogen and LMW compounds which render

pyDOM to be much more biologically labile (Goranov et al., 2020). Surprisingly, it was found that Oak 400 Fresh (1646 bio-labile formulas) is more bio-labile than its photo-irradiated counterpart (Oak 400 Photo, 1242 bio-labile formulas). However, this observation using molecular data does not agree with quantitative carbon loss results for the 10-day incubation (Oak 400 Fresh: 16% carbon loss, Oak 400 Photo: 25 % carbon loss). The observed discrepancy is because LMW compounds contribute to a large fraction of the degraded carbon in the Oak 400 pyDOM systems and LMW species are not observed following the employed PPL sample preparation and FT-ICR-MS detection. A similar discrepancy is observed when comparing Oak 400 Photo (1242 bio-labile formulas, 25% carbon loss) and Oak 650 Photo (1410 bio-labile formulas, 23% carbon loss). In contrast, Oak 650 Fresh (1364 bio-labile formulas) was observed to be less bio-labile than Oak 650 Photo (1410 bio-labile formulas) via both FT-ICR-MS and the observed quantitative carbon losses (Oak 650 Fresh: 15% carbon loss, Oak 650 Photo: 23 % carbon loss). LMW species are less abundant in the Oak 650 pyDOM systems resulting in consistent trends between the analyses. Bio-degradability trends derived from FT-ICR-MS molecular data match those from the UV-VIS data from chromophoric pyDOM (Figure S1) revealing a similar inability of UV-VIS to detect LMW compounds which do not absorb UV-VIS light. In summary, we observe a degradation of a variety of different molecular classes as well as a production of many molecules that appear to be of high biological lability. However, we caution that there are observed discrepancies among carbon loss and molecular/chromophoric data for the Oak 400 pyDOM systems, an observation that highlights the need to clearly understand methodological analytical windows when interpreting molecular and spectroscopic data.

Interestingly for all leachates, the degraded (bio-labile) molecules were not from a specific area of the vK diagrams but rather represent a broad range of H/C and O/C ratios and compound types (see Fig. S2). This variety of compound characteristics among bio-labile molecules suggests that the degradation pathway may not be from microbial consumption alone. It would be unlikely for the soil microorganisms to utilize organic matter compounds as food indiscriminately. Most interestingly, it is evident that large numbers of aromatic ($AI_{MOD} \geq 0.50$) formulas are lost, in agreement with observed losses in CDOM (Fig. S1 in the Supplement) and losses in aryl functional groups (measured by 1H NMR) reported in the parallel study (Bostick et al., 2021). ConAC were found to be resistant to bio-degradation (Bostick et al., 2021) and therefore losses of ConAC observed via FT-ICR-MS are considered an artifact due the low ionizability of ConAC and competition processes in the ESI source (Stenson et al., 2002; Patriarca et al., 2020). However, the agreement between FT-ICR-MS and other quantitative data (UV-VIS, NMR, TOC) confirms the interpretation of bulk pyDOM degradation. Approximately half of the formulas (37 – 56%) in the original pyDOM leachates are classified, using the presence-absence approach, as bio-resistant (observed before and after biotic degradation). These formulas are located in all areas of the vK diagrams (Fig. S3), showing variable oxygenation and aromaticity. The relative peak magnitudes of these formulas did not change significantly following the incubations ($R^2 > 0.95$, Fig. S9; Sleighter et al., 2012), also suggesting that a wide variety of pyDOM molecules are resistant to microbial degradation. Using the available molecular data, it is not possible to attribute the observed recalcitrance to any molecular property. Therefore, it is likely that some of these bio-resistant molecules are still bio-labile and would have degraded in due time if the incubations were sampled at later time points. Longer time series should be conducted in future studies to fully differentiate among bio-labile and bio-resistant pyDOM molecules.

The use of hydrogen-to-carbon ratio (H/C) versus molecular weight (MW) plots has also been useful in interpreting ultrahigh resolution mass spectrometry data (e.g., Gonsior et al., 2018; Powers et al., 2019; Valle et al., 2020). Such graphs are presented using the presence-absence approach in Figs. S5-8 in Sect. 3 of the Supplement. These graphics help evaluate how different types of compounds (aliphatic versus aromatic) change relative to their MW. For both Oak 400 leachates, it is clear that large aromatic molecules ($H/C < 1.5$, $MW > 550$ Da) are removed during the biotic degradation, and smaller ($300 < MW < 550$) aromatic compounds are produced. The consumption of large molecules indicates that microbes utilize extracellular enzymes to produce ROS which degrade larger molecules into smaller substrates (Billen et al., 1990). The large aromatic molecules that are being degraded into smaller ones are mainly ligninaceous and not ConAC, in agreement with the insignificant changes in BPCA data published by Bostick et al. (2021). With regards to the aliphatic molecules ($H/C > 1.5$), it is clear that molecules of a wide range of MW are degraded and produced during the incubations suggesting that MW is not a critical factor in their bio-lability. This is in apparent disagreement with the general knowledge that microbes

preferentially consume LMW substrates (e.g., Søndergaard and Middelboe, 1995). Bostick et al. (2021) also concluded that LMW substances are preferentially degraded in the incubations of pyDOM. The observed production of higher MW aliphatics suggest that the microbial incubations were still very active at the point of sampling (10 days). This additionally suggests that future studies need to evaluate the molecular composition of biotically incubated pyDOM over a longer time scale.

3.2 Composition of bio-produced organic matter

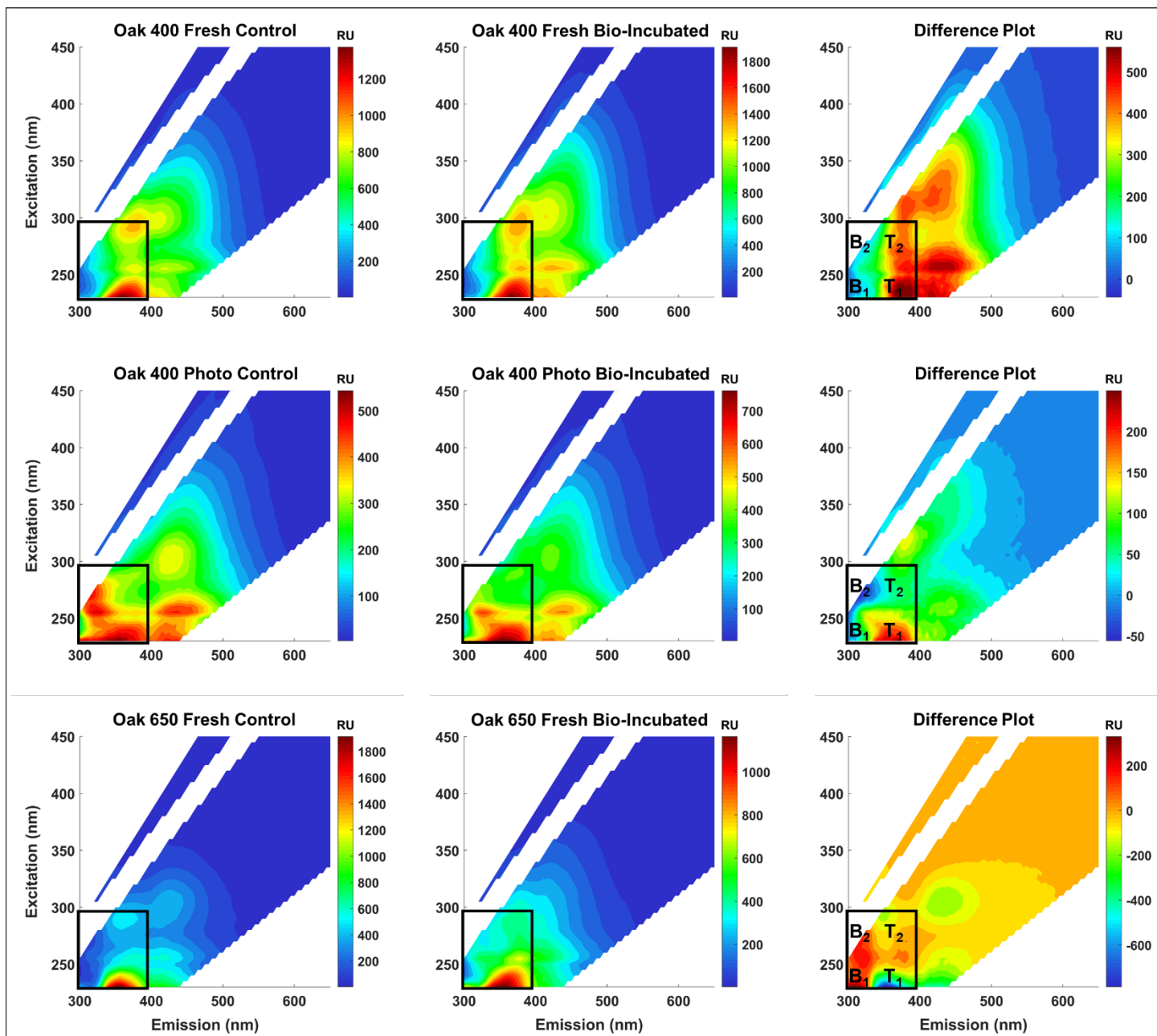
The bio-produced organic compounds can be evaluated in various ways to examine the processes that may have occurred during the incubations. Using a presence-absence approach (Sleighter et al., 2012), the bio-produced formulas of each sample are compared with those of the other samples (Table 1). No significant overlap was found (2 – 320 formulas in common, 0 – 12%) among the molecules produced in the incubated pyDOM samples. Furthermore, no significant match was found between the bio-produced formulas of incubated pyDOM and those of the sucrose control sample (63 – 94 formulas in common, 3%, Table 1). These observations indicate that the products of the incubations were vastly different for each sample and likely depend on the starting substrate. An alternative explanation is that bio-produced formulas were further altered post-exudation by ROS to result in their molecular diversification.

Table 1. Overlap of bio-produced molecular formulas among samples. The number of formulas corresponds to the formulas in common between the two samples being compared, and the percentage is relative to the total number of formulas in the two formula sets.

Sample	Oak 400 Fresh	Oak 400 Photo	Oak 650 Fresh	Oak 650 Photo
Oak 400 Fresh	-	-	-	-
Oak 400 Photo	320 (12%)	-	-	-
Oak 650 Fresh	126 (4%)	104 (5%)	-	-
Oak 650 Photo	165 (5%)	81 (3%)	2 (0%)	-
Sucrose	94 (3%)	63 (3%)	68 (3%)	83 (3%)

A significant fraction of the bio-produced organic matter was characterized as peptide-like (N-containing, $1.5 \leq H/C \leq 2.0$, $0.1 \leq O/C \leq 0.67$). This indicates that microbes convert a part of pyDOM into labile DOM (Moran et al., 2016; Vorobev et al., 2018), a process hereafter referred to as “microbial labilization”. Given that the pyDOM samples used in this study were poor in organic nitrogen, the microbes must have used the inorganic nitrogen (NH_4^+) that was provided as a nutrient and converted some or all of it into microbial biomass. Peptide-like formulas comprised 22 – 40 % of the bio-produced formulas (Table S2 in the Supplement). The results of the comparative analyses described above imply that these proteinaceous formulas are of highly variable composition. Their molecular diversity is additionally evaluated using one-way analysis of variance (ANOVA) reported in Sect. 6 of the Supplement. This statistical analysis revealed high molecular variability supporting the findings by the presence-absence comparisons presented earlier (Table 1). Collectively, these findings conclude that the microbial incubations of pyDOM created pools of new, very diverse molecules, a process hereafter referred to as “microbial diversification”. As FT-ICR-MS was performed with soft electrospray ionization with no fragmentation, the structure of the observed molecules is inferred from the elemental composition of the assigned molecular formulas. Another possibility for these N-containing molecules is that they were formed by coupling reactions among pyDOM molecules with the NH_4^+ nutrient that was added to support microbial growth (e.g., via Michael addition reactions; McKee et al., 2014).

To confirm that the bio-produced formulas were associated with proteinaceous structures and are not just N-containing compounds that coincidentally plotted in the peptide region, spectrofluorometric analysis was performed to obtain excitation-emission matrices (EEMs) of the pyDOM samples before and after bio-incubation (Fig. 2). The data for Oak 650 Photo is not reported as the produced EEM spectra were of questionable quality, and as the sample was in very limited amounts, analytical replication and quality assessment were not possible.



398
 399 **Figure 2.** Fluorescence excitation-emission matrices (EEMs) of control (left panels) and bio-incubated (middle
 400 panels) pyDOM samples. Difference spectra are shown in the right panels. The black box indicates the region
 401 where compounds of proteinaceous origin fluoresce (Coble, 1996; Coble et al., 2014), with tyrosine-like (B_1 and
 402 B_2) and tryptophan-like (T_1 and T_2) peaks labeled on the difference plots.
 403

404
 405 Proteinaceous organic matter has a highly characteristic fluorophoric signature due to the distinguishable
 406 signals of the aromatic amino acids tyrosine and tryptophan. The short Stokes' shifts of these fluorophores allow
 407 them to spectroscopically separate on the EEM plot allowing for identification of related labile substances
 408 (Wünsch et al., 2019). Other amino acids, namely histidine and phenylalanine, are also fluorophoric, but are not
 409 easily identified in EEM data of complex matrices. A practical approach to evaluate the change after the bio-
 410 incubation is to use difference plots (e.g., Hemmler et al., 2019). For all samples, strong proteinaceous signals
 411 evolve after biotic incubations indicating that molecules of autochthonous (microbial) origin are produced (Coble,
 412 1996; Coble et al., 2014). This indicated that peptide-like molecules observed using FT-ICR-MS are not
 artificially produced by coupling reactions growth (e.g., via Michael addition reactions; McKee et al., 2014) or

413 evolve due to less charge competition in the ESI source. Thus, the protein-like formulas are truly bio-produced,
414 validating the findings of the presence-absence analysis.

415 There are subtle differences among the EEMs of all control and bio-incubated samples indicative of the
416 high variability in fluorophoric content of these samples. This agrees with the observed variability in molecular
417 composition described earlier. An interesting observation is that in the two Oak 400 pyDOM incubations,
418 tyrosine-like fluorescence (peaks B₁ and B₂) decreases after biotic incubation whereas tryptophan-like
419 fluorescence (peaks T₁ and T₂) increases. In contrast, the tryptophan-like fluorophores are degraded and tyrosine-
420 like ones are produced after biotic incubation of Oak 650 Fresh pyDOM. It must be noted that there are
421 proteinaceous fluorophores (and peptide-like formulas) in the control samples resulting from the addition of the
422 microbial inoculate, but the associated fluorophores were present in low amounts. Thus, proteinaceous
423 fluorescence signals in the control samples are not unexpected. However, a decrease in proteinaceous
424 fluorophores is opposite of what is expected after significant microbial growth. Proteinaceous compounds are
425 highly bio-labile and aromatic compounds are susceptible to oxidation by ROS. Therefore, it is possible that
426 tyrosine-like fluorophores (in Oak 400 pyDOM) and tryptophan-like fluorophores (in Oak 650 pyDOM) are still
427 actively participating in bio-degradation processes as the incubations were still active at the time of sampling (10
428 days). The loss of tyrosine-like fluorophores in the Oak 400 samples, and loss of tryptophan-like fluorophores in
429 the Oak 650 Fresh sample, are indicative of different microbial physiology and exudates. The complexity of these
430 EEM spectra and the compound-specific changes observed here indicate that proteomic and/or metabolomic
431 analyses (e.g., Nalven et al., 2020) are necessary in future microbiological studies in order to fully understand the
432 changes to the molecular composition of pyDOM during biotic incubations.

433 To determine if the bio-produced formulas are from true proteins, or are from compounds with residual
434 proteinaceous fluorophores, the formulas were evaluated in the context of possible combinations of amino acids
435 that would be singly charged. Given that microbes exude large proteins (MW > 30 kDa) such as lignin
436 peroxidases, manganese peroxidases, and laccases (Higuchi, 2004), the peptide-like formulas observed by FT-
437 ICR-MS (analytical window of 200-1000 Da) may have resulted from hydrolysis of the above-mentioned
438 enzymes (or other proteinaceous exudates). If that is the case, the hydrolysates would likely have had a simple
439 oligomeric composition. To test this, the bio-produced peptide-like formulas in each sample were compared to a
440 library of 888,009 possible combinations of 20 amino acids (oligomeric sequences of 2-7 residues). Only a small
441 number of oligopeptides were identified (5 – 18 oligopeptides of 2 – 5 amino acids, Tables S2 and S3 in the
442 Supplement) which is counter to the proposed idea that hydrolysis of microbial exudates produced these newly
443 observed peptide-like formulas. Therefore, the observed bio-produced formulas may represent compounds with
444 residual proteinaceous fluorophores and are not true oligopeptides. The lack of identified oligopeptides also calls
445 into question the idea that microbial processes were solely responsible for the high variability of the bio-produced
446 organic matter observed after the microbial incubation of pyDOM.

447 To further elucidate the composition of these bio-produced N-containing substances, we re-evaluated the
448 previously published ¹H NMR data of these samples (Bostick et al., 2021) in greater detail. Additionally, the
449 connectivity between previously observed functional groups was assessed using two-dimensional ¹H-¹H total
450 correlation NMR spectroscopy (TOCSY) on a select sample. Figure 3 shows the TOCSY spectra of the bio-
451 incubated Oak 650 Fresh sample.

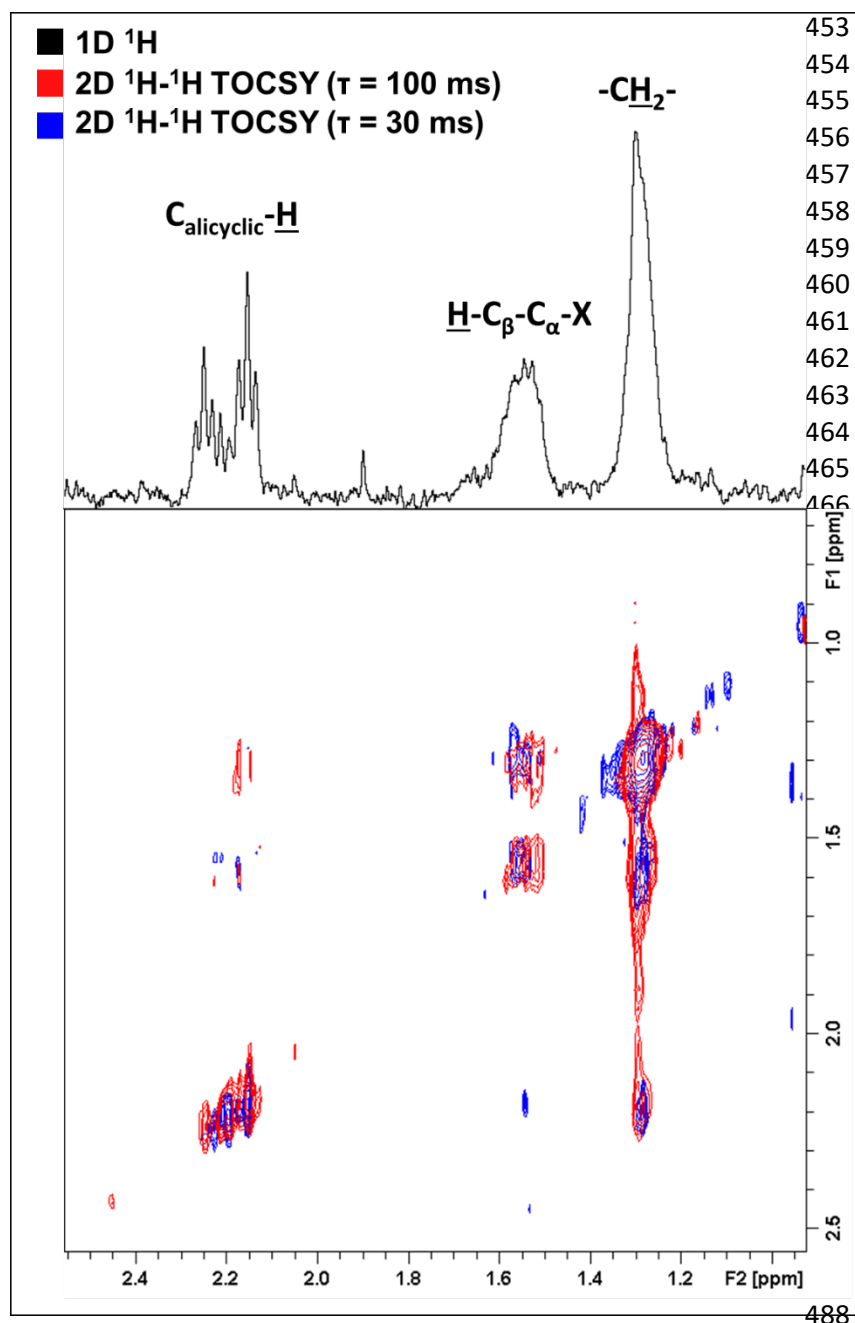


Figure 3. Two-dimensional ^1H - ^1H total correlation spectroscopy (TOCSY) NMR spectra of the bio-incubated Oak 650 Fresh sample. Short- and long-range couplings were allowed to evolve during mixing times (τ) of 30 (blue) and 100 ms (red), respectively. The 1D ^1H spectrum is shown as a projection on top (black).

There are three groups of resonances representing an alicyclic structure, a β -hydrogen to a heteroatom, and a methylene group that were found in all samples, even in the controls (although of small contributions relative to the total spectral signal). These resonances have not been previously observed in the ^1H NMR spectra of these pyDOM samples (Bostick et al., 2018; Goranov et al., 2020) indicating that they represent by-products of the microbial incubations, likely microbial biomass. In the control samples, the compounds associated with these resonances must be from the soil inoculant that was added. The three resonances are observed to be in the same coupling network indicating that they are a part of the same or similar structures. Due to the very low concentration of these samples ($3.5 - 4 \text{ mgC}\cdot\text{L}^{-1}$), the NMR analysis did not allow for a high-resolution structural elucidation, but some distinct signatures were nonetheless observed. The deshielded aliphatic peaks at $\delta = 2.1 - 2.3 \text{ ppm}$ have a complex multiplicity pattern, a characteristic feature of alicyclic structures. These are likely residual carbohydrate moieties which have lost most of their O-containing groups through various cleavage processes and their backbone $\text{C}_{\text{alicyclic}}\text{-H}$ resonances have been shifted upfield. The peak at 1.55 ppm is from β -hydrogens to a heteroatom ($\text{H-C}_{\beta}\text{-C}_{\alpha}\text{-X}$, where $\text{X} = \text{O}, \text{N}, \text{S}$), and these are known to be associated with

peptidoglycans (Spence et al., 2011). The TOCSY analysis was performed with two different mixing times ($\tau = 30$ and $\tau = 100$ ms) in order to evaluate short-range (2 – 3 bond) and long-range (4 – 6 bond) connectivities. Based on the observed couplings the observed resonances are vicinal to each other (3 bonds away). This indicates that these functional groups are closely bound in the peptidoglycan substances they likely represent.

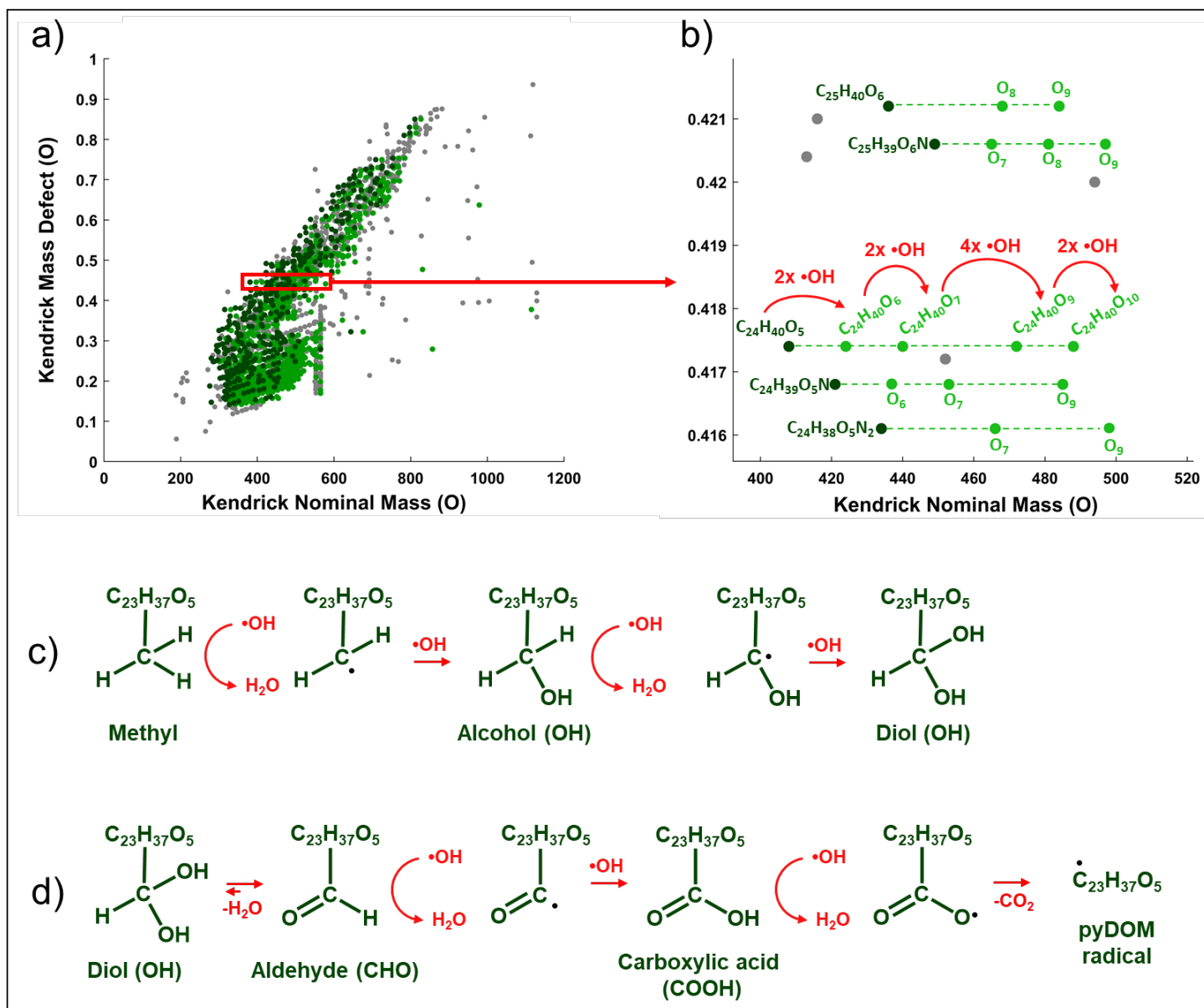
All of the assessments described above conclude that the observed biochemical processes in these pyDOM incubations are complex and difficult to unambiguously interpret. Based on our findings, we summarize that the bio-produced formulas (Figure 1) can originate from three possible sources:

- 1) exoenzymes, which microbes use to extracellularly degrade larger molecules into smaller ones (Hyde and Wood, 1997; Higuchi, 2004);
- 2) peptidoglycans, which likely leached into solution after bacterial death and cell lysis (Yavitt and Fahey, 1984); and
- 3) other metabolites and exudates involved in the physiology of the different microbes in the used consortium (e.g., signaling compounds).

The significant degradation of pyDOM and production of these biological compounds indicates that microbes successfully converted the presumably carbon-rich recalcitrant pyrogenic molecules into more labile substances, a process we define as microbial labilization. However, the fact that the observed bio-produced labile molecules are not identifiable as simple oligopeptides, and are present in significantly different composition among the four samples, suggests that this molecular diversity may not be caused by predictable biotic reactions but by random radical-driven processes. Further evidence for the random radical-driven processes comes from the observed degradation of molecules across the whole vK space (Figs. 1 and S2), which is unusual because microbes preferentially consume smaller aliphatic species (Berggren et al., 2010a,b; Kirchman, 2018).

3.3 Radical oxygenation as a potential source of molecular diversity

Microbial physiology has been associated with the production of reactive oxygen species (ROS), which have been shown to be important in the degradation of various types of organic compounds (e.g., Scully et al., 2003; McNally et al., 2005; Porcal et al., 2013; Trusiak et al., 2018; Xiao et al., 2020). Recent studies showed that radicals can degrade various types of ligninaceous molecules (Waggoner et al., 2015, 2017; Waggoner and Hatcher, 2017) suggesting that microbially induced radical reactions can target a variety of pyDOM molecules as well. While there were no ROS measurements made in this study, we have performed Kendrick mass defect (KMD) analysis of the FT-ICR-MS data (Kendrick, 1963; Hughey et al., 2001) to seek evidence for radical processes. The KMD analysis identifies formulas that differ by any repeating structural moiety (e.g., $-\text{CH}_2-$). To identify potential products of radical attacks, we have evaluated the FT-ICR-MS data in the context of oxygenation, i.e., searched the mass lists for formulas differing by one oxygen atom (addition of hydroxyl group), carbonyl group (addition of aldehydes or ketones), and carboxyl groups (Fig. 4).

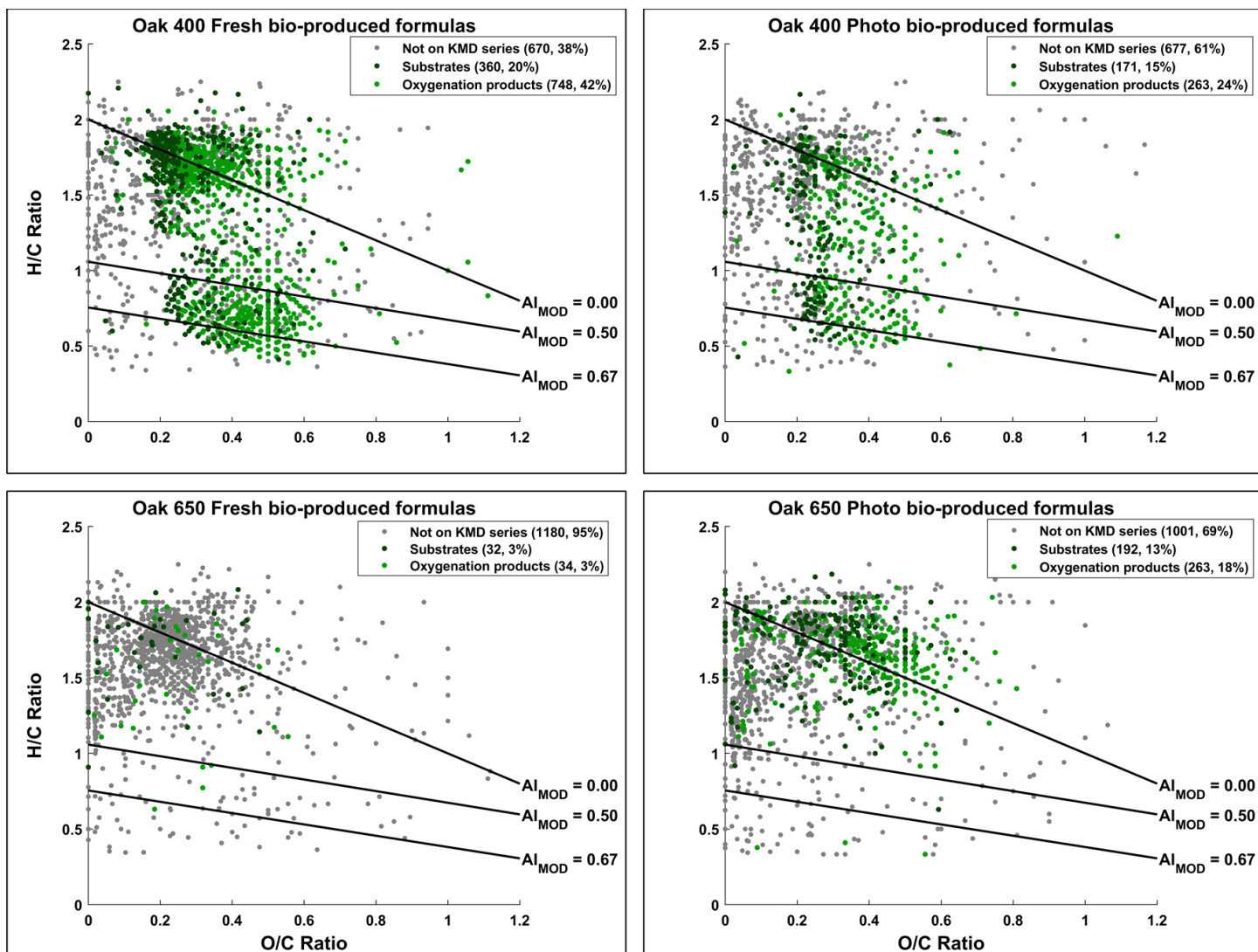


539
 540 **Figure 4.** Kendrick mass defect (KMD) analysis using oxygen (O) series of the bio-produced formulas of Oak
 541 400 Fresh pyDOM. Panel a) shows the whole KMD plot while panel b) shows an expanded region of it. Formulas
 542 not part of the O KMD series are colored in **gray**. Formulas in **dark green** are proposed substrates, and their
 543 oxygenation products are colored in **light green**. Only the molecular formulas for one of the series (KMD =
 544 0.4174 Da) are labeled while for the rest of the molecules, only the substrate formula and the number of oxygens
 545 in the oxygenation products are listed for clarity. The red arrows show the formation of the four oxygenation
 546 products of the $C_{24}H_{40}O_5$ substrate after a sequential attack by hydroxyl radicals ($\cdot OH$). Panel c) shows possible
 547 chemical reactions that can cause an increase of number of oxygens. Panel d) shows further oxidative processes
 548 involving the formation of keto and carboxyl groups which processes ultimately produce pyDOM radicals and
 549 CO_2 . The KMD plots for all samples are shown on Figs. S10-12 in the Supplement.

550
 551 The mathematics behind the KMD analysis (see Sect. 2.4) convert the mass of the molecular formula (also
 552 known as the IUPAC mass) to a “Kendrick” mass placing the formula on a scale that is specific for the selected
 553 structural moiety. On Fig. 4a, an example is shown with the KMD analysis for molecules differing by one oxygen
 554 ($-O-$). On the regular (IUPAC) mass scale, such formulas would differ by 15.994915 Da, but on the Kendrick “O”
 555 mass scale, they differ by 16 Da. The difference between the Kendrick mass (e.g., KM = 408.2876 Da) and the
 556 Kendrick nominal mass (e.g., KNM = 408 Da) is the Kendrick mass defect, KMD (i.e., KMD = 0.2876 Da).

557 Formulas with the exact same KMD differ by one or more oxygens and lie on a KMD series. Visually these
558 formulas would plot on horizontal lines on the KMD plot as indicated by the dashed lines in Fig. 4b. Taking the
559 series of $\text{KMD} = 0.4174 \text{ Da}$ as an example, the KMD evaluation shows that there are five formulas in this
560 particular KMD series that differ in number of oxygens ($\text{C}_{24}\text{H}_{40}\text{O}_{5-10}$). This implies that once $\text{C}_{24}\text{H}_{40}\text{O}_5$ is
561 produced, it acts as a substrate and the other four formulas ($\text{C}_{24}\text{H}_{40}\text{O}_{6-10}$) are produced by oxygenation (likely in
562 a sequential manner: $\text{C}_{24}\text{H}_{40}\text{O}_5 \rightarrow \text{C}_{24}\text{H}_{40}\text{O}_6 \rightarrow \text{C}_{24}\text{H}_{40}\text{O}_7 \rightarrow \text{C}_{24}\text{H}_{40}\text{O}_9 \rightarrow \text{C}_{24}\text{H}_{40}\text{O}_{10}$). Such formulas differing in
563 the number of oxygens can be formed via oxygenation by hydroxyl radical ($\bullet\text{OH}$) attacks (Waggoner et al., 2015,
564 2017; Waggoner and Hatcher, 2017). This ROS can abstract a hydrogen from C-H bonds and the hydrogen is
565 substituted with an OH-group, resulting in the formation of alcohols (C-OH) as shown in Fig. 4c. This is the
566 suggested pathway of how the oxygenation products shown in Fig. 4a and 4b have formed. Evidence for such
567 reactions will be found on the KMD plots as evolution of new molecules within the same KMD series, but with
568 a different number of oxygens. Further radical attacks would produce polyols (Fig. 4c). In the case of formation
569 of geminal diols (two alcohol groups on the same carbon atom), they can rearrange to aldehydes or ketones via
570 keto-enol tautomerism (Fig. 4d). Further radical attacks would produce carboxyl groups, which can also be
571 radically cleaved, and pyDOM radicals be formed. PyDOM radicals (as well as any other radical intermediate in
572 this pathway) can be then further paired with hydrogen radicals ($\bullet\text{H}$) from the solution, other $\bullet\text{OH}$ radicals, or
573 other radicalized pyDOM or proteinaceous species.

574 Using KMD analysis, formulas that could have been produced by oxygenation were identified and plotted
575 individually (Fig. 5). It is assumed that the smallest molecule in each series is the substrate and any molecules
576 with increasing number of oxygens are oxygenation products.



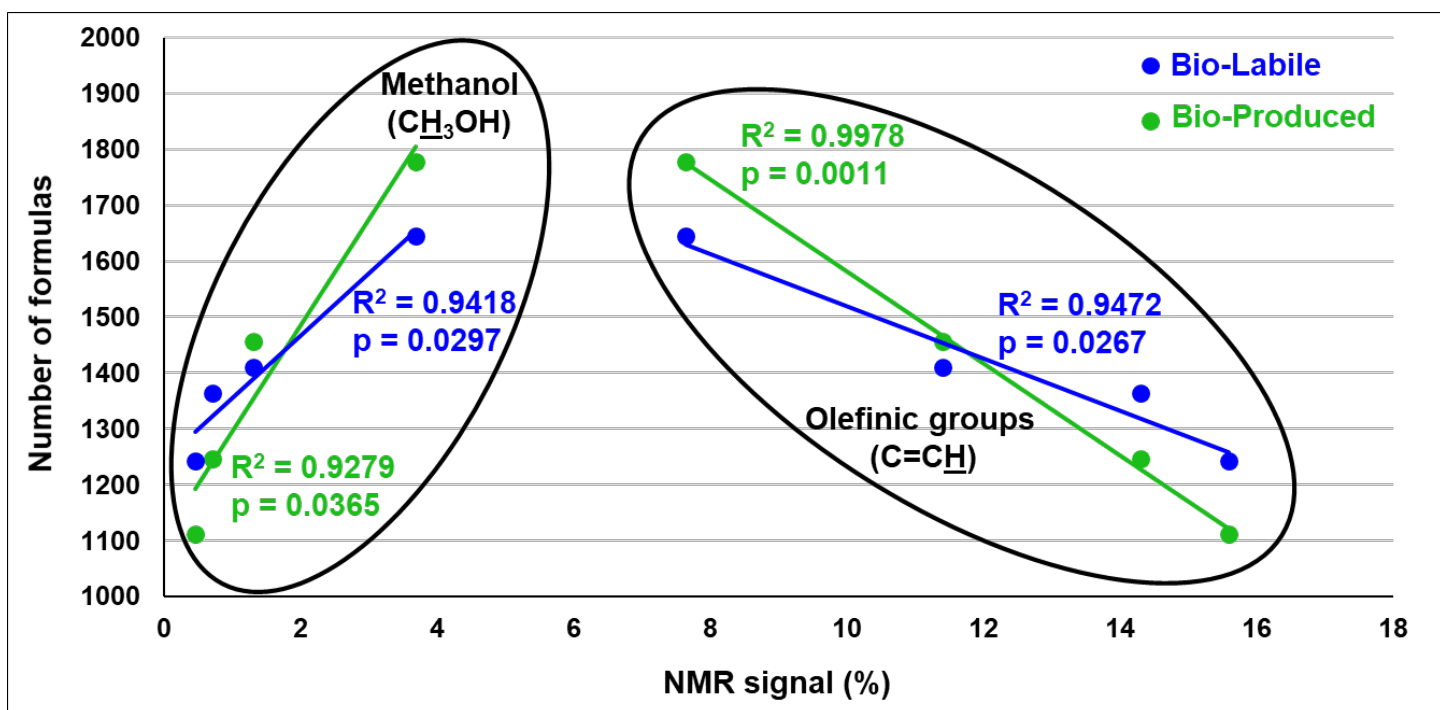
578
579 **Figure 5.** Van Krevelen diagrams showing oxygenation products among the bio-produced formulas of the four
580 incubated pyDOM samples. Formulas not part of any of the oxygenation KMD series (O, CO, or COO) are
581 colored in **gray**. Formulas in **dark green** are substrates with their oxygenation products colored in **light green**.
582 The number of formulas in each of these pools are shown in the legends (along with corresponding percentages).
583 The black lines indicate modified aromaticity index cutoffs (AI_{MOD} ; Koch and Dittmar, 2006, 2016).
584

585 KMD analysis revealed that about a third (34 – 748, 3 – 42%) of the bio-produced formulas could be
586 classified as products of oxygenation reactions, likely driven by ROS species such as the hydroxyl radical ($\bullet OH$).
587 This is in agreement with previously observed cross-linking of microbial compounds through oxidative processes
588 (Sun et al., 2017). The majority of the bio-produced formulas, however, were not found to be products of oxidation
589 as they did not lie on any of the evaluated KMD series (O, CO, or COO). Therefore, the majority of the bio-
590 produced formulas are likely formulas of exudates which were resistant to radical attacks or are formulas of
591 compounds which have already been radically coupled with other compounds to result in unrecognizable
592 molecules by the KMD analysis.

593 Additional evidence for intense radical processes in these systems is the evolution of bio-produced
594 unsaturated aliphatic compounds ($1 < H/C < 2$, $O/C < 2$) on the vK diagrams (Figs. 1 and S4). ROS can attack
595 aliphatic and aromatic compounds, open aromatic and alicyclic rings, cleave oxygen- or nitrogen-containing
596 functionalities, and produce highly aliphatic molecules, as previously observed after photo-irradiation of pyDOM
597 (Goranov et al., 2020), ConAC (Zeng et al., 2000a,b), and radical-based degradation of lignin (Waggoner et al.,
598 2015, 2017; Waggoner and Hatcher, 2017; Khatami et al., 2019a, b). ROS can also attack any of the proteinaceous

599 exudates and peptidoglycans cleaving them from many of their functional groups and converting them into the
 600 observed unsaturated aliphatic compounds. These produced aliphatic compounds could also contribute to the
 601 newly produced N-containing (“peptide-like”) compounds observed by FT-ICR-MS if they are oxygenated by
 602 ROS post-formation. However, this seems unlikely as data from the supplementary fluorescence and NMR
 603 analyses support the formation of microbial biomass. The KMD analysis shown here strongly suggests the
 604 presence of intense radical processes as formulas with increasing numbers of oxygen atoms are known to be
 605 formed following radical oxygenation (Waggoner et al., 2015, 2017; Waggoner and Hatcher, 2017). However, it
 606 must be noted that this KMD analysis does not directly prove the existence of radical processes and the suggested
 607 radical processes are speculated based only on indirect observations. Future studies need to directly test the
 608 presence of radical reactions by performing biotic incubations of pyDOM with radical quenchers as well as by
 609 quantifying radical fluxes in these microbiological systems.

610 While FT-ICR-MS peak magnitudes are a function of molecular ionizability, making it generally
 611 impossible to quantify the different bio-labile and bio-produced compounds of our study, the ultrasensitivity of
 612 this technique ensures detection of all compounds that are within the FT-ICR-MS analytical window. Here, the
 613 number of molecular formulas can be used as a quantitative measure for molecular diversity (e.g., Gurganus et
 614 al., 2015). Previously published liquid-state ¹H NMR data for the same samples (Bostick et al., 2021) provide a
 615 quantitative measure of functional group content. Significant positive and negative correlations were observed
 616 between the numbers of bio-labile and bio-produced formulas and the percent NMR spectral signal accounted for
 617 by olefinic functionalities and methanol (Fig. 6 and Table S4). These correlations suggest that the diversity of
 618 bio-degraded (bio-labile) and bio-produced molecules was related in some way with a process related to the
 619 availability of methanol (CH₃OH) and olefinic functionalities (C=C) in pyDOM.
 620



621
 622 **Figure 6.** Pearson correlation analysis between the number of **bio-labile** and **bio-produced** formulas detected by
 623 FT-ICR-MS and relative intensity (in %) of olefinic functionalities (C=C) and methanol (CH₃OH) as measured
 624 by liquid-state ¹H NMR and reported by Bostick et al. (2021). No significant correlations were found between
 625 other functional groups and the number of bio-produced or bio-labile formulas (data shown in Table S4 of the
 626 Supplement).
 627

628 Olefinic functionalities have been recently identified as important structural motifs in the composition of
 629 pyDOM and were observed to degrade in photochemical experiments likely due to their high reactivity with ROS
 630 species (Goranov et al., 2020). Although olefins are in low abundance in pyDOM (< 10%), it is likely that they

act as important intermediates in the degradative pathways of pyDOM. The olefinic bonds can be homolytically cleaved when attacked by radicals and effectively act as radical-accelerators that further propagate radical-mediated organic matter transformations. Thus, the abundance of olefins can further increase the abundance of radicals and contribute to the elevated molecular diversity resulting in the significant correlation shown in Fig. 6.

The other significant correlation between molecular diversity and NMR data is observed to be with methanol (CH₃OH), a very sharp highly distinguishable singlet at $\delta = 3.34$ ppm in ¹H NMR spectra (Gottlieb et al., 1997). As it is a common contaminant in NMR analysis, special precautions were taken to obtain ultraclean spectra (see Sect. 2.5). Methanol is a species that is naturally present in pyDOM (Bostick et al., 2018), and while it is generally considered to be toxic to microbes (Dyrda et al., 2019), there are methylotrophic bacteria and fungi (microbes of the families *methylococcaceae* and *methylobacteriaceae*) that can utilize it as a substrate (Chistoserdova et al., 2003; Kolb and Stacheter, 2013; Chistoserdova and Kalyuzhnaya, 2018). These species have been previously observed in the soil from the area where the microbial inoculum was extracted from (Khodadad et al., 2011) suggesting that the degradation of methanol may be biotic. In fact, in these samples, methanol, along with the other two measured LMW substances, acetate and formate, was almost completely degraded over the 10-day incubation (Bostick et al., 2021).

The inverse relationship between the content of methanol and molecular diversity (Fig. 6) can be interpreted in several ways. Firstly, methanol could be exhibiting toxicity to the microbes that assimilate pyDOM, as has been observed previously (Dyrda et al., 2019). This, however, is unlikely for the pyDOM systems studied here because the sample with the highest amount of methanol (Oak 400 Photo, ~3.7% CH₃OH) was the second most bio-reactive (Bostick et al., 2021). Instead, the observed significant negative correlation may be explained by the fact that methanol is a known radical-scavenger (Můčka et al., 2013). If, as we propose, the molecular diversity results from the activity of radical processes, an increasing concentration of methanol would quench ROS thereby decreasing the radical activity and limiting the molecular diversity in these systems.

4 Discussion

4.1 Multiple pathways for the alteration of pyDOM by microbes

Using a variety of analytical platforms in this and the parallel study (Bostick et al., 2021), significant quantitative and qualitative losses were observed when pyDOM was subjected to incubation with a microbial consortium collected from a site impacted by wildfires. Additionally, labile and diverse compounds were produced during these incubations. Due to the high complexity of pyDOM, the changes are not straightforward, and there are at least two degradation pathways at play: 1) degradation through microbial assimilation (consumption of pyDOM), and 2) degradation/transformation via radical-mediated reactions (e.g., oxygenation) by ROS produced from microbial exoenzymes. These two pathways are discussed in the context of degradation of pyDOM and formation of new labile and diverse molecules.

4.1.1 Molecular degradation of pyDOM

A surprising observation in this study is that there was a uniform loss of pyDOM molecules from all regions of the vK diagrams. Microbes, it is generally presumed, preferentially assimilate small non-aromatic substances such as carbohydrates, proteins, and LMW acids (Berggren et al., 2010a,b; Kirchman, 2018). Thus, the aromatic fraction of pyDOM, mainly the ConAC, are generally considered to be bio-resistant (Goldberg, 1985; Masiello, 2004). In addition to the condensed character of many of the molecules, there are significant numbers of potentially toxic organochlorine compounds, of both aliphatic and aromatic character, in pyDOM (Wozniak et al., 2020). Thus, the finding of the major biological activity in these pyDOM systems and the significant amount of carbon, including aromatic carbon, that was mineralized, is a very significant finding for the wildfire biogeochemistry community (Bostick et al., 2021).

Although pyDOM is highly heterogeneous (Wozniak et al., 2020), the observation of diverse molecular bio-degradation is not unique to it. In a recent microbial degradation study of snow DOM, Antony et al. (2017)

681 observed that both aromatic and aliphatic formulas were bio-degraded. This is likely due to microbes evolving
682 chemical mechanisms to thrive under extreme glacial conditions (Antony et al., 2016). Analogously, as there have
683 been previous prescribed fires in the area from which the microbes for this study were extracted (Johns, 2016), it
684 is also possible that our microbes had adapted to the presence of pyOM by developing mechanisms for
685 assimilating the carbon in large, complex molecules including ConAC (Judd et al., 2007).

686 While direct microbial assimilation of pyDOM compounds is certainly likely to have occurred, our
687 molecular and spectroscopic findings suggest a second degradative pathway contributing to the extensive
688 molecular alteration, and to the significant loss of carbon that was quantified in the parallel study (Bostick et al.,
689 2021). While some microbial exoenzymes operate via hydrolytic pathways (amylases, lipases, proteases,
690 cellulases, β -galactosidases, etc.), many other enzymes operate through oxidative (electron-withdrawing)
691 pathways. Examples of such enzymes are the various lignin-modifying enzymes in the peroxidase (lignin
692 peroxidases, manganese peroxidases, etc.) and phenoloxidase (e.g., laccases) families (Higuchi, 2004). Thus,
693 ROS are usually produced and involved in the microbial degradation of organic matter in the environment.

694 The bio-labile molecules in the studied pyDOM samples are of highly variable degrees of oxygenation,
695 aromaticity, and size. There were large MW compounds (MW > 550 Da) that were degraded indicating that
696 microbial exoenzymes producing ROS would have been needed to reduce the size of these large substrates into
697 smaller units that could pass through microbial cell membranes and be consumed by the biota (Sinsabaugh et al.,
698 1997; Fuchs et al., 2011; Burns et al., 2013). The presence of enzymatic compounds is confirmed by observation
699 of peptide-like compounds (FT-ICR-MS analysis) and proteinaceous fluorophores (spectrofluorometric analysis).
700 An important finding is that a preferential degradation of ConAC of smaller MW was observed (Bostick et al.,
701 2021). As small ConAC (i.e., oxygenated polycondensed aromatic hydrocarbons) are known to be toxic (e.g.,
702 Idowu et al., 2019), it is unlikely that they were directly consumed by the microbes. Oxygenated polycondensed
703 aromatic hydrocarbons are highly susceptible to attacks by ROS, which is likely how they were degraded in these
704 samples. Thus, we speculate that microbes are most likely not directly consuming the smaller ConAC, but rather,
705 smaller ConAC are degraded indirectly via ROS oxidation. Furthermore, ROS can oxygenate pyDOM with
706 various functional groups (e.g., hydroxy, aldehyde/keto, carboxyl), and can also cleave functional groups (e.g.,
707 methoxy functionalities), open aromatic rings, and completely mineralize compounds to inorganic carbon (CO,
708 CO₂, HCO₃⁻ and CO₃²⁻) as shown on Fig. 4. ROS have been previously shown to be very important in pyDOM
709 photochemistry (Ward et al., 2014; Fu et al., 2016; Wang et al., 2020), and we speculate that they play an
710 important role in the microbial degradation of pyDOM as well.

711 More indirect evidence for radical species involvement is provided by the peptidoglycan molecules
712 produced during the pyDOM incubations. Peptidoglycan molecules are generally large (Vollmer et al., 2008) and
713 would not be detected as singly-charged ions using FT-ICR-MS (analytical window covering only m/z 200-1000).
714 The hydrolytic products of peptidoglycans though (small oligopeptides) would be observed. Very few peptide
715 sequences (5 – 18 oligopeptides of 2 – 5 residues) were identified among the bio-produced formulas indicating
716 that such hydrolysates did not exist in the samples at the time of measurement. However, if there were abundant
717 radical reactions occurring in the system, as we suggest, it is very possible that these hydrolysates were altered
718 into unrecognizable organic structures that would still be classified as “peptide-like” but would have different
719 molecular composition than the predicted linear peptide sequences. It is also possible that instead of peptidoglycan
720 hydrolysis followed by consecutive oxygenation, ROS directly cleaved the peptidoglycans into smaller non-linear
721 substances of peptide-like molecular composition.

722 It must be noted that the results of our study were acquired using negative-mode ESI which is only
723 effective for electronegative (carboxyl-rich, hydroxyl-rich) compounds (Stenson et al., 2002; Patriarca et al.,
724 2020). Thus, the trends of degradation and labilization are skewed to fit this criterion and do not provide a
725 complete overview of all molecules that are bio-labile or bio-produced. Future studies should employ positive-
726 mode ESI and/or different ionization sources (such as atmospheric pressure photoionization) to better elucidate
727 the molecular degradability of pyDOM.

4.1.2 Labilization and Diversification of pyDOM

The production of labile unrecognizable biological substances during these incubations correlates well with previous findings showing the formation of thousands of new biological compounds during biotic incubations unrelated to microbial metabolic pathways (Lechtenfeld et al., 2015; Wienhausen et al., 2017; Patriarca et al., 2021). There was no significant overlap among the bio-produced formulas of the four pyDOM samples (2 – 320 formulas in common, 0 – 12%). Insignificant numbers of bio-produced formulas from pyDOM were also found in the bio-produced formulas of an incubation of sucrose with the same soil microbes (63 – 94 formulas, 3%). This indicates that microbes diversified the composition of the incubated pyDOM.

The observed diversity of bio-produced formulas can be explained by a scenario wherein the microbes secreted molecules whose identities differed depending on the growth medium and/or food source, yielding high variability among bio-produced formulas after the incubation of pyDOM. Additionally, it is possible that different microbial species (different bacteria, fungi, archaea, etc.) have proliferated in response to the sample-specific pyDOM composition, yielding different microbial populations growing during each different incubation, sequentially producing different bio-produced compounds (Fitch et al., 2018). Another possible explanation for the observed diversification is the presence of ROS-driven oxygenation processes. ROS are known to be key species in the consumption of organic matter by microbes. Microbes can only consume small molecules that could pass through their cell membranes (Sinsabaugh et al., 1997; Fuchs et al., 2011; Burns et al., 2013). Thus, to utilize large molecules as food, microbes produce exoenzymes which generate ROS extracellularly (Hyde and Wood, 1997; Higuchi, 2004). These ROS then degrade the large molecules into smaller ones that are utilized as food. Though not directly proven to exist in this study, many of the observed trends in FT-ICR-MS, NMR, and fluorescence data suggest the presence of radicals which diversify the composition of the bio-produced formulas.

Our finding of extreme molecular diversity contrasts with previous observations in a study by Lechtenfeld et al. (2015) evaluating the molecular composition of microbially produced DOM. In their study, marine microbes were supplied with two different substrates (glucose and glutamic acid; and a mixture of oligosaccharides and oligopeptides), and a significant overlap (67 – 69 %) in the bio-produced organic matter was observed. The difference in observations between the work presented in this manuscript and by Lechtenfeld et al. (2015) is likely caused by a large difference in the composition of the pyDOM substrates relative to those in the Lechtenfeld et al. (2015) study. While the four pyDOM samples used here are highly heterogeneous to one another (Goranov et al., 2020; Wozniak et al., 2020), the substrates by Lechtenfeld et al. (2015) were of much higher similarity (glucose, glutamic acid, oligosaccharides and oligopeptides). Another possible reason is that due to different physiology the soil microbes used here may be producing more diverse biomass than the marine microbes used by Lechtenfeld et al. (2015). It is likely that aquatic microbes have a much different degradation strategy than soil microbes. As soils are far less rich in labile molecules, it is possible that soil microbes have evolved to produce much higher fluxes of ROS to degrade the more recalcitrant soil organic matter into consumable substrates, which can also explain the larger dissimilarity in bio-produced organic molecules after the incubations of pyDOM.

An important observation using the H/C versus MW plots (Fig. S5) was that the bio-produced compounds after incubation of pyDOM were of various MW. Thus, it is likely that the microbial biomass produced during the incubation is radically coupled with ambient pyDOM molecules or their biochemical remnants. Radical coupling been recently proposed as an important process in marine DOM cycling (Hach et al., 2020). In that study, when isotopically ¹³C-labeled organisms were incubated with oceanic surface waters, microbially produced compounds were quickly coupled to the ambient marine DOM molecules. This “recombination” process occurred within hours of the production of microbial exudates, followed by the observation of a highly diversified DOM pool. This process is likely driven by radical coupling reactions, and such pathways have also been observed in incubations in the presence of sunlight (Sun et al., 2017). Another possible explanation is that chemically reactive species, such as quinones, reacted with microbially produced compounds or the NH₄⁺ nutrient via nucleophile-driven reactions (such as the Michael addition; McKee et al., 2014) to produce highly diverse pools of molecules after each incubation.

Our results are also compared to previous work by Waggoner et al. (2017) where a ligninaceous sample was treated with three different ROS: hydroxyl radical (\bullet OH), singlet oxygen (1 O₂), and superoxide (O₂⁻). Each

781 different radical degraded a specific pool of ligninaceous compounds, which showed that different ROS can
782 degrade a variety of types of organic matter. However, there was a significant overlap observed between the three
783 pools of molecules that were degraded (Waggoner et al., 2017) indicating that degradation pathways solely based
784 on ROS attacks are still ordered. Thus, because ROS on their own do not produce completely diversified
785 molecular pools, the combination of the two possible pathways (consumption and ROS degradation) must have
786 occurred to produce the great variability in the bio-produced microbial biomass observed in our study.

787 Collectively, our results indicate that pyDOM can be both directly consumed by biota and secondarily
788 degraded by ROS-driven processes. These pathways could not be explored at a mechanistic level in the current
789 study, and we suggest that future studies focus on employing more specialized analytical techniques (e.g., genetic
790 sequencing, ROS quantification) for deconvoluting the complexity of the bio-degradation of pyDOM.

791 **4.2 Implications for the cycling of pyDOM in the environment**

792
793
794 The present study provides a detailed evaluation of the compounds that microbes degrade and produce in
795 samples mimicking pyDOM in hydrologically dynamic systems such as riverine and groundwater systems. This
796 work brings new knowledge regarding the properties and degradability of pyDOM and challenges the
797 conventional idea that pyDOM is stable towards biotic degradation. Several studies have already shown that
798 pyrogenic substances have soluble DOM components (Hockaday et al., 2007; Mukherjee and Zimmerman, 2013;
799 Wagner et al., 2017; Bostick et al., 2018) and that more soluble components are produced with environmental
800 aging (Abiven et al., 2011; Ascough et al., 2011; Roebuck et al., 2017; Quan et al., 2020). The experiments
801 presented here, in parallel with Bostick et al. (2021), show that a large portion of pyDOM can be remineralized
802 (bio-degraded to CO₂) without priming (Guenet et al., 2010; Bianchi, 2011), which indicates that pyrogenic
803 molecules may be far less resistant to bio-degradation than previously presumed.

804 The involvement of pyDOM within the global carbon cycle is complex, and for many biogeochemical
805 processes, poorly understood. There is a growing body of literature showing that significant amounts of ConAC
806 are solubilized and exported to the global ocean (Dittmar et al., 2012; Jaffé et al., 2013; Wang et al., 2016;
807 Marques et al., 2017; Jones et al., 2020) suggesting constant global leaching of pyDOM in riverine systems from
808 pyOM in soils. The global riverine flux of pyDOM is estimated using the recently reported global flux of ConAC
809 (18 Tg·C·y⁻¹) and scaled using a factor of 7.5 as proposed by Bostick et al. (2018) to be 135 Tg·C·y⁻¹, a value
810 that is much lower than the estimated annual pyDOM production and seepage flux of 1440 Tg·C·y⁻¹ (Bostick et
811 al., 2018). In addition to the implied 91% loss of carbon during riverine export, a recent study also reported that
812 the stable carbon isotopic signature ($\delta^{13}\text{C}$) of oceanic ConAC is not terrestrial, but rather, marine-like (Wagner et
813 al., 2019). This suggests that either all riverine-exported ConAC are being mineralized before they reach the
814 global ocean or ConAC are chemically altered significantly to change their $\delta^{13}\text{C}$ isotopic signature (Jones et al.,
815 2020). Microbial and photochemical processes have been found to transform DOM with characteristic terrestrial
816 DOM composition (compounds with lower H/C and higher O/C ratios) into compounds having characteristics of
817 marine-derived DOM (compounds with higher H/C, lower O/C ratios; Rossel et al., 2013). Thus, pyDOM may
818 simply be losing its diagnostic molecular and isotopic terrestrial-like fingerprints during riverine export due to a
819 variety of degradative post-production processes, and the observed molecular transformations in our study are
820 likely one of them.

821 The cycling of organic matter in the environment has always been an enigma, and there has been a long-
822 standing effort to explain the fate of terrestrial DOM (including pyDOM) in the global ocean (Hedges et al.,
823 1997). In a previous manuscript evaluating the photochemical transformation of pyDOM (Goranov et al., 2020),
824 we suggested that biotic consumption of photo-degradation products of pyDOM (“small aliphatic compounds”)
825 could result in the formation of marine-like DOM. This hypothesis was tested by comparing our incubation
826 products (the bio-produced formulas) to FT-ICR-MS formulas of an estuarine transect of the Elizabeth River, VA
827 (Sleighter and Hatcher, 2008) and another ten oceanic DOM samples (reported in Sect. 5 of the Supplement). A
828 significant number of common formulas was observed in these comparisons (193 – 308 common formulas, 8 –
829 18% overlap) confirming the hypothesis that bio-incubation of pyDOM can produce marine-like DOM. The
830 observed common formulas were not condensed and 81 – 192 of them (42 – 70%) were of molecular composition

831 attributed to carboxyl-rich alicyclic molecules (CRAM) per Hertkorn et al. (2006). These results indicate that
832 biotic incubations of pyDOM (regardless of photo-irradiation) can contribute to some of the molecules observed
833 in oceanic environments. The fact that some of these molecules were observed in both surface and abyssal oceanic
834 DOM indicate that some pyDOM bio-degradation products may be sequestered into the deep ocean as refractory
835 DOM.

836 The observed bio-produced labile formulas in our study do not appear to be commonly observed in other
837 environmental samples. This is likely because these labile molecules are part of the fast-cycling, labile DOM pool
838 per Hansell's model (Hansell and Carlson, 2015), and are quickly depleted in the natural environment. This
839 parallels the findings of a recently published study (Hach et al., 2020) observing that microbially produced
840 molecules are extremely labile and are, within hours, broken down and recombined with ambient DOM
841 molecules. The closed laboratory systems in our study may have enabled the observation of these highly labile
842 molecules whereas in the natural environment they would have been quickly transformed, diluted, or mineralized
843 to inorganic carbon resulting in their removal from analytical detection. The richness in nitrogen and peptide-like
844 character of the bio-produced molecules we observe suggest greater potential lability (Hach et al., 2020), and it
845 is likely that the by-products of biotic degradation of pyDOM are readily incorporated into microbial food webs.
846 This is consistent with the idea that terrestrial DOM is either mineralized to CO₂ or incorporated into food webs
847 (Berggren et al., 2010a; Ward et al., 2013; Fasching et al., 2014). It is also consistent with the suggestion that the
848 majority of organic nitrogen in the oceans is derived from microbial peptidoglycans (McCarthy et al., 1997, 1998;
849 Simpson et al., 2011) and with observations of nitrogen from peptidoglycans in soil and sedimentary porewater
850 systems (Schulten and Schnitzer, 1998; Hu et al., 2018, 2020).

851 The production of highly variable and diverse bio-produced molecules is likely a contributing factor to
852 the large complexity of natural organic matter (Hertkorn et al., 2007; Hawkes et al., 2018). Our observed bio-
853 produced molecules likely contribute to the highly variable microbial exometabolomes observed previously
854 (Antón et al., 2013; Watrous et al., 2013; Romano et al., 2014) and stimulate further questions about pyDOM's
855 function and fate within the global carbon and nitrogen cycles. In this study, we have used soil microbes, as the
856 corresponding degradation by-products can be observed in both soil, groundwater, and partially in the upstream
857 sections of rivers. Therefore, it would be critical to perform further studies with different microbial consortia
858 (riverine, estuarine, marine, etc.) to fully understand the biological degradation of pyDOM in different
859 environments. Additionally, the observed evidence for two possible degradative pathways (consumption and ROS
860 degradation) indicates that these pyDOM incubations are extremely complex systems. Future microbiological
861 studies must aim to investigate these pathways further by designing radical quenching experiments (to test for
862 presence/absence of radical oxygenation pathways) as well as employ bio-analytical techniques (e.g., genetic
863 sequencing; Nalven et al., 2020) for assessing what microbes are responsible for the labilization and
864 diversification of pyDOM.

866 5 Conclusions

867
868 This study probing the molecular changes occurring after biotic degradation of pyDOM revealed that soil
869 microbes can effectively recycle and transform a significant portion of pyDOM molecules into labile microbial
870 biomass. After the 10-day incubations, it appears that a wide range of pyDOM molecules, both aromatic and
871 aliphatic, were degraded, forming a highly diverse pool of compounds, including N-containing compounds with
872 proteinaceous signatures and a peptidoglycan-like backbone. These observations are consistent with the previous
873 identification of nitrogen from peptidoglycans in soils and oceans. These bio-produced compounds were highly
874 specific for each pyDOM sample which was concluded by observing very few common bio-produced molecular
875 formulas among incubated samples. The observed molecular labilization and diversification have implications
876 for the biogeochemistry of pyDOM as we show that microbial reworking of pyDOM can contribute to the large
877 complexity and variability of natural organic matter. This study reveals that 1) pyDOM can be a medium for
878 microbial growth, and 2) previously considered "recalcitrant" pyrogenic molecules can be broken down and the
879 carbon and nitrogen therein can be incorporated into microbial food webs. This study suggests that pyDOM is a
880 much more active component in the global carbon and nitrogen cycles and that some non-condensed pyDOM

degradation products have an oceanic fate. Therefore, future studies need to further evaluate the bio-degradability of pyDOM with microbial consortia of different environments, as well as in the context of wetted soils, groundwater processes, cycling within the riverine and marine water columns, and other aspects of the global carbon and nitrogen cycles.

Data Availability. Research Data associated with this article can be accessed at <https://doi.org/10.17632/kjkhy3tfys.1>

Competing Interests. The authors declare that they have no conflict of interest.

Author Contributions. Conceptualization, A.I.G., A.S.W., K.W.B., A.R.Z., S.M., P.G.H.; Investigation, K.W.B., A.I.G.; Formal analysis, A.I.G.; Writing – Original Draft Preparation, A.I.G.; Writing – Review & Editing, A.I.G., A.S.W., K.W.B., A.R.Z., S.M., P.G.H.; Funding Acquisition, A.S.W., A.R.Z., S.M., P.G.H.

Acknowledgments. We thank Rachel L. Sleighter for providing the estuarine and oceanic FT-ICR-MS data. We also thank Isaiah Ruhl, Dr. Deepti Varma, and Dr. Ravi Garimella for assistance during instrumental analyses at the COSMIC facility (Old Dominion University), and Dow Van Arnam (University of Florida) for design and construction of the biochar pyrolyzer and solar simulator. This project was funded by National Science Foundation (Geobiology and Low-Temperature Geochemistry Program, proposal numbers EAR-1451452 and EAR-1451367) and the Frank Batten Endowment Fund to Dr. Patrick G. Hatcher (Old Dominion University). Additionally, we appreciate Old Dominion University for supporting Aleksandar I. Goranov through the Dominion Fellowship. Lastly, we would like to express our gratitude to the editor and referees for their time and feedback in improving this manuscript.

References

- Aboudi, M., Jeffrey, W. H., Ghiglione, J. F., Pujo-Pay, M., Oriol, L., Sempéré, R., Charrière, B., and Joux, F.: Effects of photochemical transformations of dissolved organic matter on bacterial metabolism and diversity in three contrasting coastal sites in the Northwestern Mediterranean Sea during summer, *Microbial Ecology*, 55, 344-357, <https://doi.org/10.1007/s00248-007-9280-8>, 2008.
- Abiven, S., Hengartner, P., Schneider, M. P. W., Singh, N., and Schmidt, M. W. I.: Pyrogenic carbon soluble fraction is larger and more aromatic in aged charcoal than in fresh charcoal, *Soil Biology & Biochemistry*, 43, 1615-1617, <https://doi.org/10.1016/j.soilbio.2011.03.027>, 2011.
- Antón, J., Lucio, M., Peña, A., Cifuentes, A., Brito-Echeverría, J., Moritz, F., Tziotis, D., López, C., Urdiain, M., Schmitt-Kopplin, P., and Rosselló-Móra, R.: High metabolomic microdiversity within co-occurring isolates of the extremely halophilic bacterium *Salinibacter ruber*, *PLoS ONE*, 8, 1-14, <https://doi.org/10.1371/journal.pone.0064701>, 2013.
- Antony, R., Sanyal, A., Kapse, N., Dhakephalkar, P. K., Thamban, M., and Nair, S.: Microbial communities associated with Antarctic snow pack and their biogeochemical implications, *Microbiological Research*, 192, 192-202, <https://doi.org/10.1016/j.micres.2016.07.004>, 2016.
- Antony, R., Willoughby, A. S., Grannas, A. M., Catanzano, V., Sleighter, R. L., Thamban, M., Hatcher, P. G., and Nair, S.: Molecular insights on dissolved organic matter transformation by supraglacial microbial communities, *Environmental Science & Technology*, 51, 4328-4337, <https://doi.org/10.1021/acs.est.6b05780>, 2017.
- Antony, R., Willoughby, A. S., Grannas, A. M., Catanzano, V., Sleighter, R. L., Thamban, M., and Hatcher, P. G.: Photo-biochemical transformation of dissolved organic matter on the surface of the coastal East Antarctic ice sheet, *Biogeochemistry*, 141, 229-247, <https://doi.org/10.1007/s10533-018-0516-0>, 2018.
- Ascough, P. L., Bird, M. I., Francis, S. M., Thornton, B., Midwood, A. J., Scott, A. C., and Apperley, D.: Variability in oxidative degradation of charcoal: Influence of production conditions and environmental

930 exposure, *Geochimica et Cosmochimica Acta*, 75, 2361-2378, <https://doi.org/10.1016/j.gca.2011.02.002>,
931 2011.

932 Bao, H., Niggemann, J., Luo, L., Dittmar, T., and Kao, S.-J.: Aerosols as a source of dissolved black carbon to
933 the ocean, *Nature Communications*, 8, 1-7, <https://doi.org/10.1038/s41467-017-00437-3>, 2017.

934 Bax, A., and Davis, D. G.: MLEV-17-based two-dimensional homonuclear magnetization transfer spectroscopy,
935 *Journal of Magnetic Resonance*, 65, 355-360, [https://doi.org/10.1016/0022-2364\(85\)90018-6](https://doi.org/10.1016/0022-2364(85)90018-6), 1985.

936 Benner, R., and Biddanda, B.: Photochemical transformations of surface and deep marine dissolved organic
937 matter: Effects on bacterial growth, *Limnology and Oceanography*, 43, 1373-1378,
938 <https://doi.org/10.4319/lo.1998.43.6.1373>, 1998.

939 Berggren, M., Laudon, H., Haei, M., Ström, L., and Jansson, M.: Efficient aquatic bacterial metabolism of
940 dissolved low-molecular-weight compounds from terrestrial sources, *The ISME Journal*, 4, 408-416,
941 <https://doi.org/10.1038/ismej.2009.120>, 2010a.

942 Berggren, M., Ström, L., Laudon, H., Karlsson, J., Jonsson, A., Giesler, R., Bergström, A.-K., and Jansson, M.:
943 Lake secondary production fueled by rapid transfer of low molecular weight organic carbon from
944 terrestrial sources to aquatic consumers, *Ecology Letters*, 13, 870-880, <https://doi.org/10.1111/j.1461-0248.2010.01483.x>, 2010b.

946 Bianchi, T. S.: The role of terrestrially derived organic carbon in the coastal ocean: A changing paradigm and the
947 priming effect, *Proceedings of the National Academy of Sciences of the United States of America*, 108,
948 19473–19481, <https://doi.org/10.1073/pnas.1017982108>, 2011.

949 Billen, G., Servais, P., and Becquevort, S.: Dynamics of bacterioplankton in oligotrophic and eutrophic aquatic
950 environments: Bottom-up or top-down control?, *Hydrobiologia*, 207, 37-42,
951 <https://doi.org/10.1007/BF00041438>, 1990.

952 Bostick, K. W., Zimmerman, A. R., Wozniak, A. S., Mitra, S., and Hatcher, P. G.: Production and composition
953 of pyrogenic dissolved organic matter from a logical series of laboratory-generated chars, *Frontiers in*
954 *Earth Science*, 6, 1-14, <https://doi.org/10.3389/feart.2018.00043>, 2018.

955 Bostick, K. W., Zimmerman, A. R., Goranov, A. I., Mitra, S., Hatcher, P. G., and Wozniak, A. S.: Biolability of
956 fresh and photodegraded pyrogenic dissolved organic matter from laboratory-prepared chars, *Journal of*
957 *Geophysical Research: Biogeosciences*, 126, 1-17, <https://doi.org/10.1029/2020JG005981>, 2021. Bostick,
958 K. W., Zimmerman, A. R., Goranov, A. I., Mitra, S., Hatcher, P. G., and Wozniak, A. S.: Photolability of
959 pyrogenic dissolved organic matter from a thermal series of laboratory-prepared chars, *Science of The*
960 *Total Environment*, 724, 1-9, <https://doi.org/10.1016/j.scitotenv.2020.138198>, 2020.

961 Burns, R. G., DeForest, J. L., Marxsen, J., Sinsabaugh, R. L., Stromberger, M. E., Wallenstein, M. D., Weintraub,
962 M. N., and Zoppini, A.: Soil enzymes in a changing environment: Current knowledge and future
963 directions, *Soil Biology & Biochemistry*, 58, 216-234, <https://doi.org/10.1016/j.soilbio.2012.11.009>,
964 2013.

965 Chen, M., and Jaffé, R.: Photo- and bio-reactivity patterns of dissolved organic matter from biomass and soil
966 leachates and surface waters in a subtropical wetland, *Water Research*, 61, 181-190,
967 <https://doi.org/10.1016/j.watres.2014.03.075>, 2014.

968 Chistoserdova, L., Chen, S.-W., Lapidus, A., and Lidstrom, M. E.: Methylotrophy in *Methylobacterium*
969 *extorquens* AM1 from a genomic point of view, *Journal of Bacteriology*, 185, 2980-2987,
970 <https://doi.org/10.1128/JB.185.10.2980-2987.2003>, 2003.

971 Chistoserdova, L., and Kalyuzhnaya, M. G.: Current trends in methylotrophy, *Trends in Microbiology*, 26, 703-
972 714, <https://doi.org/10.1016/j.tim.2018.01.011>, 2018.

973 Coble, P. G.: Characterization of marine and terrestrial DOM in seawater using excitation-emission matrix
974 spectroscopy, *Marine Chemistry*, 51, 325-346, [https://doi.org/10.1016/0304-4203\(95\)00062-3](https://doi.org/10.1016/0304-4203(95)00062-3), 1996.

975 Coble, P. G., Lead, J., Baker, A., Reynolds, D. M., and Spencer, R. G. M.: *Aquatic Organic Matter Fluorescence*,
976 Cambridge University Press, New York, NY, 2014.

977 Coppola, A. I., Seidel, M., Ward, N. D., Viviroli, D., Nascimento, G. S., Haghypour, N., Revels, B. N., Abiven,
978 S., Jones, M. W., Richey, J. E., Eglinton, T. I., Dittmar, T., and Schmidt, M. W. I.: Marked isotopic

979 variability within and between the Amazon River and marine dissolved black carbon pools, *Nature*
980 *Communications*, 10, 1-8, <https://doi.org/10.1038/s41467-019-11543-9>, 2019.

981 D'Andrilli, J., Fischer, S. J., and Rosario-Ortiz, F. L.: Advancing critical applications of high resolution mass
982 spectrometry for DOM assessments: Re-engaging with mass spectral principles, limitations, and data
983 analysis, *Environmental Science & Technology*, 54, 11654-11656,
984 <https://doi.org/10.1021/acs.est.0c04557>, 2020.

985 Dittmar, T., Koch, B., Hertkorn, N., and Kattner, G.: A simple and efficient method for the solid-phase extraction
986 of dissolved organic matter (SPE-DOM) from seawater, *Limnology and Oceanography: Methods*, 6, 230-
987 235, <https://doi.org/10.4319/lom.2008.6.230>, 2008.

988 Dittmar, T., and Paeng, J.: A heat-induced molecular signature in marine dissolved organic matter, *Nature*
989 *Geoscience*, 2, 175-179, <https://doi.org/10.1038/ngeo440>, 2009.

990 Dittmar, T., de Rezende, C. E., Manecki, M., Niggemann, J., Coelho Ovalle, A. R., Stubbins, A., and Bernardes,
991 M. C.: Continuous flux of dissolved black carbon from a vanished tropical forest biome, *Nature*
992 *Geoscience*, 5, 618-622, <https://doi.org/10.1038/ngeo1541>, 2012.

993 Druffel, E.: Comments on the importance of black carbon in the global carbon cycle, *Marine Chemistry*, 92, 197-
994 200, <https://doi.org/10.1016/j.marchem.2004.06.026>, 2004.

995 Dyrda, G., Boniewska-Bernacka, E., Man, D., Barchiewicz, K., and Słota, R.: The effect of organic solvents on
996 selected microorganisms and model liposome membrane, *Molecular Biology Reports*, 46, 3225-3232,
997 <https://doi.org/10.1007/s11033-019-04782-y>, 2019.

998 Fasching, C., Behounek, B., Singer, G. A., and Battin, T. J.: Microbial degradation of terrigenous dissolved
999 organic matter and potential consequences for carbon cycling in brown-water streams, *Scientific Reports*,
000 4, 1-7, <https://doi.org/10.1038/srep04981>, 2014.

001 Fitch, A., Orland, C., Willer, D., Emilson, E. J. S., and Tanentzap, A. J.: Feasting on terrestrial organic matter:
002 Dining in a dark lake changes microbial decomposition, *Global change biology*, 24, 5110-5122,
003 <https://doi.org/10.1111/gcb.14391>, 2018.

004 Fu, H. Y., Liu, H. T., Mao, J. D., Chu, W. Y., Li, Q. L., Alvarez, P. J. J., Qu, X. L., and Zhu, D. Q.: Photochemistry
005 of dissolved black carbon released from biochar: Reactive oxygen species generation and
006 phototransformation, *Environmental Science & Technology*, 50, 1218-1226,
007 <https://doi.org/10.1021/acs.est.5b04314>, 2016.

008 Fuchs, G., Boll, M., and Heider, J.: Microbial degradation of aromatic compounds - from one strategy to four,
009 *Nature Reviews Microbiology*, 9, 803-816, <https://doi.org/10.1038/nrmicro2652>, 2011.

010 Goldberg, E. D.: *Black carbon in the environment: Properties and distribution*, J. Wiley, New York, NY, 1985.

011 Gonsior, M., Hertkorn, N., Hinman, N., Dvorski, S. E., Harir, M., Cooper, W. J., and Schmitt-Kopplin, P.:
012 Yellowstone hot springs are organic chemodiversity hot spots, *Scientific Reports*, 8, 1-13,
013 <https://doi.org/10.1038/s41598-018-32593-x>, 2018.

014 Goranov, A. I., Wozniak, A. S., Bostick, K. W., Zimmerman, A. R., Mitra, S., and Hatcher, P. G.: Photochemistry
015 after fire: Structural transformations of pyrogenic dissolved organic matter elucidated by advanced
016 analytical techniques, *Geochimica et Cosmochimica Acta*, 290, 271-292,
017 <https://doi.org/10.1016/j.gca.2020.08.030>, 2020.

018 Gottlieb, H. E., Kotlyar, V., and Nudelman, A.: NMR chemical shifts of common laboratory solvents as trace
019 impurities, *The Journal of Organic Chemistry*, 62, 7512-7515, <https://doi.org/10.1021/Jo971176v>, 1997.

020 Green, S. A., and Blough, N. V.: Optical absorption and fluorescence properties of chromophoric dissolved
021 organic matter in natural waters, *Limnology and Oceanography*, 39, 1903-1916,
022 <https://doi.org/10.4319/lo.1994.39.8.1903>, 1994.

023 Guenet, B., Danger, M., Abbadie, L., and Lacroix, G.: Priming effect: Bridging the gap between terrestrial and
024 aquatic ecology, *Ecology*, 91, 2850-2861, <https://doi.org/10.1890/09-1968.1>, 2010.

025 Gurganus, S. C., Wozniak, A. S., and Hatcher, P. G.: Molecular characteristics of the water soluble organic matter
026 in size-fractionated aerosols collected over the North Atlantic Ocean, *Marine Chemistry*, 170, 37-48,
027 <https://doi.org/10.1016/j.marchem.2015.01.007>, 2015.

- 028 Hach, P. F., Marchant, H. K., Krupke, A., Riedel, T., Meier, D. V., Lavik, G., Holtappels, M., Dittmar, T., and
029 Kuypers, M. M. M.: Rapid microbial diversification of dissolved organic matter in oceanic surface waters
030 leads to carbon sequestration, *Scientific Reports*, 10, 1-10, <https://doi.org/10.1038/s41598-020-69930-y>,
031 2020.
- 032 Hansell, D. A., and Carlson, C. A.: *Biogeochemistry of marine dissolved organic matter*, Second ed., Academic
033 Press, Amsterdam, 712 pp., 2015.
- 034 Hawkes, J. A., Patriarca, C., Sjöberg, P. J. R., Tranvik, L. J., and Bergquist, J.: Extreme isomeric complexity of
035 dissolved organic matter found across aquatic environments, *Limnology and Oceanography Letters*, 3,
036 21-30, <https://doi.org/10.1002/lo2.10064>, 2018.
- 037 Hedges, J. I., Keil, R. G., and Benner, R.: What happens to terrestrial organic matter in the ocean?, *Organic*
038 *Geochemistry*, 27, 195-212, [https://doi.org/10.1016/S0146-6380\(97\)00066-1](https://doi.org/10.1016/S0146-6380(97)00066-1), 1997.
- 039 Helms, J. R., Stubbins, A., Ritchie, J. D., Minor, E. C., Kieber, D. J., and Mopper, K.: Absorption spectral slopes
040 and slope ratios as indicators of molecular weight, source, and photobleaching of chromophoric dissolved
041 organic matter, *Limnology and Oceanography*, 53, 955-969, <https://doi.org/10.4319/lo.2008.53.3.0955>,
042 2008.
- 043 Hemmler, D., Gonsior, M., Powers, L. C., Marshall, J. W., Rychlik, M., Taylor, A. J., and Schmitt-Kopplin, P.:
044 Simulated sunlight selectively modifies Maillard reaction products in a wide array of chemical reactions,
045 *Chemistry*, 25, 13208-13217, <https://doi.org/10.1002/chem.201902804>, 2019.
- 046 Hertkorn, N., Benner, R., Frommberger, M., Schmitt-Kopplin, P., Witt, M., Kaiser, K., Kettrup, A., and Hedges,
047 J. I.: Characterization of a major refractory component of marine dissolved organic matter, *Geochimica*
048 *et Cosmochimica Acta*, 70, 2990-3010, <https://doi.org/10.1016/j.gca.2006.03.021>, 2006.
- 049 Hertkorn, N., Ruecker, C., Meringer, M., Gugisch, R., Frommberger, M., Perdue, E., Witt, M., and Schmitt-
050 Kopplin, P.: High-precision frequency measurements: Indispensable tools at the core of the molecular-
051 level analysis of complex systems, *Analytical and Bioanalytical Chemistry*, 389, 1311-1327,
052 <https://doi.org/10.1007/s00216-007-1577-4>, 2007.
- 053 Higuchi, T.: Microbial degradation of lignin: Role of lignin peroxidase, manganese peroxidase, and laccase,
054 *Proceedings of the Japan Academy, Series B*, 80, 204-214, <https://doi.org/10.2183/pjab.80.204>, 2004.
- 055 Hockaday, W. C., Grannas, A. M., Kim, S., and Hatcher, P. G.: Direct molecular evidence for the degradation
056 and mobility of black carbon in soils from ultrahigh-resolution mass spectral analysis of dissolved organic
057 matter from a fire-impacted forest soil, *Organic Geochemistry*, 37, 501-510,
058 <https://doi.org/10.1016/j.orggeochem.2005.11.003>, 2006.
- 059 Hockaday, W. C., Grannas, A. M., Kim, S., and Hatcher, P. G.: The transformation and mobility of charcoal in a
060 fire-impacted watershed, *Geochimica et Cosmochimica Acta*, 71, 3432-3445,
061 <https://doi.org/10.1016/j.gca.2007.02.023>, 2007.
- 062 Hockaday, W. C., Purcell, J. M., Marshall, A. G., Baldock, J. A., and Hatcher, P. G.: Electrospray and
063 photoionization mass spectrometry for the characterization of organic matter in natural waters: A
064 qualitative assessment, *Limnology and Oceanography: Methods*, 7, 81-95,
065 <https://doi.org/10.4319/lom.2009.7.81>, 2009.
- 066 Hu, Y., Zheng, Q., Zhang, S., Noll, L., and Wanek, W.: Significant release and microbial utilization of amino
067 sugars and D-amino acid enantiomers from microbial cell wall decomposition in soils, *Soil Biology &*
068 *Biochemistry*, 123, 115-125, <https://doi.org/10.1016/j.soilbio.2018.04.024>, 2018.
- 069 Hu, Y., Zheng, Q., Noll, L., Zhang, S., and Wanek, W.: Direct measurement of the *in situ* decomposition of
070 microbial-derived soil organic matter, *Soil Biology & Biochemistry*, 141, 1-10,
071 <https://doi.org/10.1016/j.soilbio.2019.107660>, 2020.
- 072 Hughey, C. A., Hendrickson, C. L., Rodgers, R. P., Marshall, A. G., and Qian, K.: Kendrick mass defect spectrum:
073 a compact visual analysis for ultrahigh-resolution broadband mass spectra, *Analytical Chemistry*, 73,
074 4676-4681, <https://doi.org/10.1021/ac010560w>, 2001.
- 075 Hyde, S. M., and Wood, P. M.: A mechanism for production of hydroxyl radicals by the brown-rot fungus
076 *Coniophora Puteana*: Fe(III) reduction by cellobiose dehydrogenase and Fe(II) oxidation at a distance
077 from the hyphae, *Microbiology*, 143, 259-266, <https://doi.org/10.1099/00221287-143-1-259>, 1997.

- 078 Idowu, O., Semple, K. T., Ramadass, K., O'Connor, W., Hansbro, P., and Thavamani, P.: Beyond the obvious:
079 Environmental health implications of polar polycyclic aromatic hydrocarbons, *Environ Int*, 123, 543-557,
080 <https://doi.org/10.1016/j.envint.2018.12.051>, 2019.
- 081 Jaffé, R., Ding, Y., Niggemann, J., Vähätalo, A. V., Stubbins, A., Spencer, R. G. M., Campbell, J., and Dittmar,
082 T.: Global charcoal mobilization from soils via dissolution and riverine transport to the oceans, *Science*,
083 340, 345-347, <https://doi.org/10.1126/science.1231476>, 2013.
- 084 Johns, G: Austin Cary Forest Prescribed Burn (33/8S/21E), School of Forest Resources and Conservation,
085 UF/IFAS, Prescribed Burn Prescription 721, 1-5, 2016
- 086 Jones, M. W., Coppola, A. I., Santín, C., Dittmar, T., Jaffé, R., Doerr, S. H., and Quine, T. A.: Fires prime
087 terrestrial organic carbon for riverine export to the global oceans, *Nature Communications*, 11, 1-8,
088 <https://doi.org/10.1038/s41467-020-16576-z>, 2020.
- 089 Judd, K. E., Crump, B. C., and Kling, G. W.: Bacterial responses in activity and community composition to photo-
090 oxidation of dissolved organic matter from soil and surface waters, *Aquatic Sciences*, 69, 96-107,
091 <https://doi.org/10.1007/s00027-006-0908-4>, 2007.
- 092 Kendrick, E.: A mass scale based on $\text{CH}_2 = 14.0000$ for high resolution mass spectrometry of organic compounds,
093 *Analytical Chemistry*, 35, 2146-2154, <https://doi.org/10.1021/ac60206a048>, 1963.
- 094 Khatami, S., Deng, Y., Tien, M., and Hatcher, P. G.: Formation of water-soluble organic matter through fungal
095 degradation of lignin, *Organic Geochemistry*, 135, 64-70,
096 <https://doi.org/10.1016/j.orggeochem.2019.06.004>, 2019a.
- 097 Khatami, S., Deng, Y., Tien, M., and Hatcher, P. G.: Lignin contribution to aliphatic constituents of humic acids
098 through fungal degradation, *Journal of Environmental Quality*, 48, 1565-1570,
099 <https://doi.org/10.2134/jeq2019.01.0034>, 2019b.
- 100 Khodadad, C. L. M., Zimmerman, A. R., Green, S. J., Uthandi, S., and Foster, J. S.: Taxa-specific changes in soil
101 microbial community composition induced by pyrogenic carbon amendments, *Soil Biology &*
102 *Biochemistry*, 43, 385-392, <https://doi.org/10.1016/j.soilbio.2010.11.005>, 2011.
- 103 Kieber, D. J., McDaniel, J., and Mopper, K.: Photochemical source of biological substrates in sea water:
104 Implications for carbon cycling, *Nature*, 341, 637-639, <https://doi.org/10.1038/341637a0>, 1989.
- 105 Kim, S., Kramer, R. W., and Hatcher, P. G.: Graphical method for analysis of ultrahigh-resolution broadband
106 mass spectra of natural organic matter, the van Krevelen diagram, *Analytical Chemistry*, 75, 5336-5344,
107 <https://doi.org/10.1021/ac034415p>, 2003.
- 108 Kirchman, D. L.: Processes in microbial ecology, Second ed., Oxford University Press, 1-318 pp., 2018.
- 109 Klevit, R. E.: Improving two-dimensional NMR spectra by t_1 ridge subtraction, *Journal of Magnetic Resonance*,
110 62, 551-555, [https://doi.org/10.1016/0022-2364\(85\)90227-6](https://doi.org/10.1016/0022-2364(85)90227-6), 1985.
- 111 Koch, B. P., and Dittmar, T.: From mass to structure: An aromaticity index for high-resolution mass data of
112 natural organic matter, *Rapid Communications in Mass Spectrometry*, 20, 926-932,
113 <https://doi.org/10.1002/rcm.2386>, 2006.
- 114 Koch, B. P., Dittmar, T., Witt, M., and Kattner, G.: Fundamentals of molecular formula assignment to ultrahigh
115 resolution mass data of natural organic matter, *Analytical Chemistry*, 79, 1758-1763,
116 <https://doi.org/10.1021/ac061949s>, 2007.
- 117 Koch, B. P., and Dittmar, T.: From mass to structure: An aromaticity index for high-resolution mass data of
118 natural organic matter (Erratum), *Rapid Communications in Mass Spectrometry*, 30, 1,
119 <https://doi.org/10.1002/rcm.7433>, 2016.
- 120 Kolb, S., and Stacheter, A.: Prerequisites for amplicon pyrosequencing of microbial methanol utilizers in the
121 environment, *Front Microbiol*, 4, 1-12, <https://doi.org/10.3389/fmicb.2013.00268>, 2013.
- 122 Kothawala, D. N., Murphy, K. R., Stedmon, C. A., Weyhenmeyer, G. A., and Tranvik, L. J.: Inner filter correction
123 of dissolved organic matter fluorescence, *Limnology and Oceanography: Methods*, 11, 616-630,
124 <https://doi.org/10.4319/lom.2013.11.616>, 2013.
- 125 Kujawinski, E. B., and Behn, M. D.: Automated analysis of electrospray ionization Fourier transform ion
126 cyclotron resonance mass spectra of natural organic matter, *Analytical Chemistry*, 78, 4363-4373,
127 <https://doi.org/10.1021/ac0600306>, 2006.

- 128 Kuzyakov, Y., Subbotina, I., Chen, H., Bogomolova, I., and Xu, X.: Black carbon decomposition and
129 incorporation into soil microbial biomass estimated by ^{14}C labeling, *Soil Biology & Biochemistry*, 41,
130 210-219, <https://doi.org/10.1016/j.soilbio.2008.10.016>, 2009.
- 131 Kuzyakov, Y., Bogomolova, I., and Glaser, B.: Biochar stability in soil: Decomposition during eight years and
132 transformation as assessed by compound-specific ^{14}C analysis, *Soil Biology & Biochemistry*, 70, 229-
133 236, <https://doi.org/10.1016/j.soilbio.2013.12.021>, 2014.
- 134 Lechtenfeld, O. J., Hertkorn, N., Shen, Y., Witt, M., and Benner, R.: Marine sequestration of carbon in bacterial
135 metabolites, *Nature Communications*, 6, 1-8, <https://doi.org/10.1038/ncomms7711>, 2015.
- 136 Lehmann, J.: A handful of carbon, *Nature*, 447, 143-144, <https://doi.org/10.1038/447143a>, 2007.
- 137 Li, M., Bao, F., Zhang, Y., Sheng, H., Chen, C., and Zhao, J.: Photochemical aging of soot in the aqueous phase:
138 Release of dissolved black carbon and the formation of $^1\text{O}_2$, *Environmental Science & Technology*, 53,
139 12311-12319, <https://doi.org/10.1021/acs.est.9b02773>, 2019.
- 140 Lindell, M. J., Granéli, W., and Tranvik, L. J.: Enhanced bacterial growth in response to photochemical
141 transformation of dissolved organic matter, *Limnology and Oceanography*, 40, 195-199,
142 <https://doi.org/10.4319/lo.1995.40.1.0195>, 1995.
- 143 Liu, M., Mao, X.-a., Ye, C., Huang, H., Nicholson, J. K., and Lindon, J. C.: Improved WATERGATE pulse
144 sequences for solvent suppression in NMR spectroscopy, *Journal of Magnetic Resonance*, 132, 125-129,
145 <https://doi.org/10.1006/jmre.1998.1405>, 1998.
- 146 Marques, J. S. J., Dittmar, T., Niggemann, J., Almeida, M. G., Gomez-Saez, G. V., and Rezende, C. E.: Dissolved
147 black carbon in the headwaters-to-ocean continuum of Paraíba Do Sul River, Brazil, *Frontiers in Earth
148 Science*, 5, 1-12, <https://doi.org/10.3389/feart.2017.00011>, 2017.
- 149 Masiello, C. A., and Druffel, E. R. M.: Black carbon in deep-sea sediments, *Science*, 280, 1911-1913,
150 <https://doi.org/10.1126/science.280.5371.1911>, 1998.
- 151 Masiello, C. A.: New directions in black carbon organic geochemistry, *Marine Chemistry*, 92, 201-213,
152 <https://doi.org/10.1016/j.marchem.2004.06.043>, 2004.
- 153 McCarthy, M., Pratum, T., Hedges, J., and Benner, R.: Chemical composition of dissolved organic nitrogen in
154 the ocean, *Nature*, 390, 150-154, <https://doi.org/10.1038/36535>, 1997.
- 155 McCarthy, M. D., Hedges, J. I., and Benner, R.: Major bacterial contribution to marine dissolved organic nitrogen,
156 *Science*, 281, 231-234, <https://doi.org/10.1126/science.281.5374.231>, 1998.
- 157 McKee, G. A., Kobiela, M. E., and Hatcher, P. G.: Effect of Michael adduction on peptide preservation in natural waters,
158 *Environmental Science: Processes & Impacts*, 16, 2087-2097, [10.1039/C4EM00075G](https://doi.org/10.1039/C4EM00075G), 2014.
- 159 McNally, A. M., Moody, E. C., and McNeill, K.: Kinetics and mechanism of the sensitized photodegradation of
160 lignin model compounds, *Photochem. Photobiol. Sci.*, 4, 268-274, <https://doi.org/10.1039/b416956e>,
161 2005.
- 162 Miller, M. P., Simone, B. E., McKnight, D. M., Cory, R. M., Williams, M. W., and Boyer, E. W.: New light on a
163 dark subject: Comment, *Aquatic Sciences*, 72, 269-275, <https://doi.org/10.1007/s00027-010-0130-2>,
164 2010.
- 165 Moran, M. A., and Covert, J. S.: Photochemically mediated linkages between dissolved organic matter and
166 bacterioplankton, in: *Aquatic Ecosystems*, edited by: Findlay, S. E. G., and Sinsabaugh, R. L., Academic
167 Press, Burlington, 243-262, 2003.
- 168 Moran, M. A., Kujawinski, E. B., Stubbins, A., Fatland, R., Aluwihare, L. I., Buchan, A., Crump, B. C.,
169 Dorrestein, P. C., Dyhrman, S. T., Hess, N. J., Howe, B., Longnecker, K., Medeiros, P. M., Niggemann,
170 J., Obernosterer, I., Repeta, D. J., and Waldbauer, J. R.: Deciphering ocean carbon in a changing world,
171 *Proceedings of the National Academy of Sciences of the United States of America*, 113, 3143-3151,
172 [10.1073/pnas.1514645113](https://doi.org/10.1073/pnas.1514645113), 2016.
- 173 Múčka, V., Bláha, P., Čuba, V., and Červenák, J.: Influence of various scavengers of $\bullet\text{OH}$ radicals on the radiation
174 sensitivity of yeast and bacteria, *International Journal of Radiation Biology*, 89, 1045-1052,
175 <https://doi.org/10.3109/09553002.2013.817702>, 2013.
- 176 Mukherjee, A., Zimmerman, A. R., and Harris, W.: Surface chemistry variations among a series of laboratory-
177 produced biochars, *Geoderma*, 163, 247-255, <https://doi.org/10.1016/j.geoderma.2011.04.021>, 2011.

- 178 Mukherjee, A., and Zimmerman, A. R.: Organic carbon and nutrient release from a range of laboratory-produced
179 biochars and biochar-soil mixtures, *Geoderma*, 193-194, 122-130,
180 <https://doi.org/10.1016/j.geoderma.2012.10.002>, 2013.
- 181 Murphy, K. R., Butler, K. D., Spencer, R. G. M., Stedmon, C. A., Boehme, J. R., and Aiken, G. R.: Measurement
182 of dissolved organic matter fluorescence in aquatic environments: An interlaboratory comparison,
183 *Environmental Science & Technology*, 44, 9405-9412, <https://doi.org/10.1021/es102362t>, 2010.
- 184 Murphy, K. R.: A note on determining the extent of the water Raman peak in fluorescence spectroscopy, *Applied*
185 *Spectroscopy*, 65, 233-236, <https://doi.org/10.1366/10-06136>, 2011.
- 186 Murphy, K. R., Stedmon, C. A., Graeber, D., and Bro, R.: Fluorescence spectroscopy and multi-way techniques.
187 PARAFAC, *Analytical Methods*, 5, 6541-6882, <https://doi.org/10.1039/c3ay41160e>, 2013.
- 188 Nalven, S. G., Ward, C. P., Payet, J. P., Cory, R. M., Kling, G. W., Sharpton, T. J., Sullivan, C. M., and Crump,
189 B. C.: Experimental metatranscriptomics reveals the costs and benefits of dissolved organic matter photo-
190 alteration for freshwater microbes, *Environmental Microbiology*, 22, 3505-3521,
191 <https://doi.org/10.1111/1462-2920.15121>, 2020.
- 192 Obernosterer, I., and Benner, R.: Competition between biological and photochemical processes in the
193 mineralization of dissolved organic carbon, *Limnology and Oceanography*, 49, 117-124,
194 <https://doi.org/10.4319/lo.2004.49.1.0117>, 2004.
- 195 Patriarca, C., Balderrama, A., Može, M., Sjöberg, P. J. R., Bergquist, J., Tranvik, L. J., and Hawkes, J. A.:
196 Investigating the ionization of dissolved organic matter by electrospray ionization, *Analytical Chemistry*,
197 92, 14210-14218, <https://doi.org/10.1021/acs.analchem.0c03438>, 2020.
- 198 Patriarca, C., Sedano-Núñez, V. T., Garcia, S. L., Bergquist, J., Bertilsson, S., Sjöberg, P. J. R., Tranvik, L. J.,
199 and Hawkes, J. A.: Character and environmental lability of cyanobacteria-derived dissolved organic
200 matter, *Limnology and Oceanography*, 66, 496-509, <https://doi.org/10.1002/lno.11619>, 2021.
- 201 Porcal, P., Dillon, P. J., and Molot, L. A.: Photochemical production and decomposition of particulate organic
202 carbon in a freshwater stream, *Aquatic Sciences*, 75, 469-482, [https://doi.org/10.1007/s00027-013-0293-](https://doi.org/10.1007/s00027-013-0293-8)
203 8, 2013.
- 204 Powers, L. C., Hertkorn, N., McDonald, N., Schmitt-Kopplin, P., Del Vecchio, R., Blough, N. V., and Gonsior,
205 M.: *Sargassum sp.* act as a large regional source of marine dissolved organic carbon and polyphenols,
206 *Global Biogeochemical Cycles*, 33, 1423-1439, <https://doi.org/10.1029/2019GB006225>, 2019.
- 207 Qi, Y., Fu, W., Tian, J., Luo, C., Shan, S., Sun, S., Ren, P., Zhang, H., Liu, J., Zhang, X., and Wang, X.: Dissolved
208 black carbon is not likely a significant refractory organic carbon pool in rivers and oceans, *Nature*
209 *Communications*, 11, 1-11, <https://doi.org/10.1038/s41467-020-18808-8>, 2020.
- 210 Qualls, R. G., and Richardson, C. J.: Factors controlling concentration, export, and decomposition of dissolved
211 organic nutrients in the Everglades of Florida, *Biogeochemistry*, 62, 197-229,
212 <https://doi.org/10.1023/A:1021150503664>, 2003.
- 213 Quan, G., Fan, Q., Zimmerman, A. R., Sun, J., Cui, L., Wang, H., Gao, B., and Yan, J.: Effects of laboratory
214 biotic aging on the characteristics of biochar and its water-soluble organic products, *Journal of Hazardous*
215 *Materials*, 382, 1-9, <https://doi.org/10.1016/j.jhazmat.2019.121071>, 2020.
- 216 Reisser, M., Purves, R. S., Schmidt, M. W. I., and Abiven, S.: Pyrogenic carbon in soils: A literature-based
217 inventory and a global estimation of its content in soil organic carbon and stocks, *Frontiers in Earth*
218 *Science*, 4, 1-14, <https://doi.org/10.3389/feart.2016.00080>, 2016.
- 219 Riedel, T., Zark, M., Vähätalo, A. V., Niggemann, J., Spencer, R. G. M., Hernes, P. J., and Dittmar, T.: Molecular
220 signatures of biogeochemical transformations in dissolved organic matter from ten world rivers, *Frontiers*
221 *in Earth Science*, 4, 1-16, <https://doi.org/10.3389/feart.2016.00085>, 2016.
- 222 Roebuck, J. A., Podgorksi, D. C., Wagner, S., and Jaffé, R.: Photodissolution of charcoal and fire-impacted soil
223 as a potential source of dissolved black carbon in aquatic environments, *Organic Geochemistry*, 112, 16-
224 21, <https://doi.org/10.1016/j.orggeochem.2017.06.018>, 2017.
- 225 Romano, S., Dittmar, T., Bondarev, V., Weber, R. J. M., Viant, M. R., and Schulz-Vogt, H. N.: Exo-metabolome
226 of *Pseudovibrio sp.* FO-BEG1 analyzed by ultra-high resolution mass spectrometry and the effect of
227 phosphate limitation, *PLoS ONE*, 9, 1-11, <https://doi.org/10.1371/journal.pone.0096038>, 2014.

- Rossel, P. E., Vähätalo, A. V., Witt, M., and Dittmar, T.: Molecular composition of dissolved organic matter from a wetland plant (*Juncus effusus*) after photochemical and microbial decomposition (1.25 yr): Common features with deep sea dissolved organic matter, *Organic Geochemistry*, 60, 62-71, <https://doi.org/10.1016/j.orggeochem.2013.04.013>, 2013.
- Santín, C., Doerr, S. H., Preston, C. M., and Gonzalez-Rodriguez, G.: Pyrogenic organic matter production from wildfires: A missing sink in the global carbon cycle, *Global change biology*, 21, 1621-1633, <https://doi.org/10.1111/gcb.12800>, 2015.
- Santín, C., Doerr, S. H., Merino, A., Bryant, R., and Loader, N. J.: Forest floor chemical transformations in a boreal forest fire and their correlations with temperature and heating duration, *Geoderma*, 264, 71-80, <https://doi.org/10.1016/j.geoderma.2015.09.021>, 2016.
- Santín, C., Doerr, S. H., Merino, A., Bucheli, T. D., Bryant, R., Ascough, P., Gao, X., and Masiello, C. A.: Carbon sequestration potential and physicochemical properties differ between wildfire charcoals and slow-pyrolysis biochars, *Scientific Reports*, 7, 1-11, <https://doi.org/10.1038/s41598-017-10455-2>, 2017.
- Schmidt, M. W. I., and Noack, A. G.: Black carbon in soils and sediments: Analysis, distribution, implications, and current challenges, *Global Biogeochemical Cycles*, 14, 777-793, <https://doi.org/10.1029/1999GB001208>, 2000.
- Schneider, M. P. W., Hilf, M., Vogt, U. F., and Schmidt, M. W. I.: The benzene polycarboxylic acid (BPCA) pattern of wood pyrolyzed between 200 °C and 1000 °C, *Organic Geochemistry*, 41, 1082-1088, <https://doi.org/10.1016/j.orggeochem.2010.07.001>, 2010.
- Schulten, H. R., and Schnitzer, M.: The chemistry of soil organic nitrogen: A review, *Biology and fertility of soils*, 26, 1-15, <https://doi.org/10.1007/s003740050335>, 1998.
- Scully, N. M., Cooper, W. J., and Tranvik, L. J.: Photochemical effects on microbial activity in natural waters: The interaction of reactive oxygen species and dissolved organic matter, *FEMS Microbiology Ecology*, 46, 353-357, [https://doi.org/10.1016/s0168-6496\(03\)00198-3](https://doi.org/10.1016/s0168-6496(03)00198-3), 2003.
- Simpson, A. J., McNally, D. J., and Simpson, M. J.: NMR spectroscopy in environmental research: From molecular interactions to global processes, *Progress in Nuclear Magnetic Resonance Spectroscopy*, 58, 97-175, <https://doi.org/10.1016/j.pnmrs.2010.09.001>, 2011.
- Sinsabaugh, R. L., Findlay, S., Franchini, P., and Fischer, D.: Enzymatic analysis of riverine bacterioplankton production, *Limnology and Oceanography*, 42, 29-38, <https://doi.org/10.4319/lo.1997.42.1.0029>, 1997.
- Skjemstad, J., Reicosky, D. C., Wilts, A., and McGowan, J.: Charcoal carbon in U.S. agricultural soils, *Soil Science Society of America Journal*, 66, 1249-1255, <https://doi.org/10.2136/sssaj2002.1249>, 2002.
- Sleighter, R. L., and Hatcher, P. G.: Molecular characterization of dissolved organic matter (DOM) along a river to ocean transect of the lower Chesapeake Bay by ultrahigh resolution electrospray ionization Fourier transform ion cyclotron resonance mass spectrometry, *Marine Chemistry*, 110, 140-152, [10.1016/j.marchem.2008.04.008](https://doi.org/10.1016/j.marchem.2008.04.008), 2008.
- Sleighter, R. L., McKee, G. A., Liu, Z., and Hatcher, P. G.: Naturally present fatty acids as internal calibrants for Fourier transform mass spectra of dissolved organic matter, *Limnology and Oceanography: Methods*, 6, 246-253, <https://doi.org/10.4319/lom.2008.6.246>, 2008.
- Sleighter, R. L., Chen, H., Wozniak, A. S., Willoughby, A. S., Caricasole, P., and Hatcher, P. G.: Establishing a measure of reproducibility of ultrahigh-resolution mass spectra for complex mixtures of natural organic matter, *Analytical Chemistry*, 84, 9184-9191, <https://doi.org/10.1021/ac3018026>, 2012.
- Smith, C. R., Hatcher, P. G., Kumar, S., and Lee, J. W.: Investigation into the sources of biochar water-soluble organic compounds and their potential toxicity on aquatic microorganisms, *ACS Sustainable Chemistry & Engineering*, 4, 2550-2558, <https://doi.org/10.1021/acssuschemeng.5b01687>, 2016.
- Søndergaard, M., and Middelboe, M.: A cross-system analysis of labile dissolved organic carbon, *Marine Ecology Progress Series*, 118, 283-294, <https://doi.org/10.3354/meps118283>, 1995.
- Spence, A., Simpson, A. J., McNally, D. J., Moran, B. W., McCaul, M. V., Hart, K., Paull, B., and Kelleher, B. P.: The degradation characteristics of microbial biomass in soil, *Geochimica et Cosmochimica Acta*, 75, 2571-2581, <https://doi.org/10.1016/j.gca.2011.03.012>, 2011.

- 277 Stenson, A. C., William, M., Marshall, A. G., and Cooper, W. T.: Ionization and fragmentation of humic
278 substances in electrospray ionization Fourier transform-ion cyclotron resonance mass spectrometry,
279 *Analytical Chemistry*, 74, 4397-4409, 2002.
- 280 Stubbins, A., Spencer, R. G. M., Chen, H. M., Hatcher, P. G., Mopper, K., Hernes, P. J., Mwamba, V. L.,
281 Mangangu, A. M., Wabakanghanzi, J. N., and Six, J.: Illuminated darkness: Molecular signatures of
282 Congo River dissolved organic matter and its photochemical alteration as revealed by ultrahigh precision
283 mass spectrometry, *Limnology and Oceanography*, 55, 1467-1477, 10.4319/lo.2010.55.4.1467, 2010.
- 284 Stubbins, A., Niggemann, J., and Dittmar, T.: Photo-lability of deep ocean dissolved black carbon,
285 *Biogeosciences*, 9, 1661-1670, <https://doi.org/10.5194/bg-9-1661-2012>, 2012.
- 286 Sun, L., Xu, C., Zhang, S., Lin, P., Schwehr, K. A., Quigg, A., Chiu, M.-H., Chin, W.-C., and Santschi, P. H.:
287 Light-induced aggregation of microbial exopolymeric substances, *Chemosphere*, 181, 675-681,
288 <https://doi.org/10.1016/j.chemosphere.2017.04.099>, 2017.
- 289 Trusiak, A., Treibergs, L., Kling, G., and Cory, R.: The controls of iron and oxygen on hydroxyl radical (\bullet OH)
290 production in soils, *Soil Systems*, 3, 1-23, <https://doi.org/10.3390/soilsystems3010001>, 2018.
- 291 Valle, J., Harir, M., Gonsior, M., Enrich-Prast, A., Schmitt-Kopplin, P., Bastviken, D., and Hertkorn, N.:
292 Molecular differences between water column and sediment pore water SPE-DOM in ten Swedish boreal
293 lakes, *Water Research*, 170, 1-11, <https://doi.org/10.1016/j.watres.2019.115320>, 2020.
- 294 Van Krevelen, D. W.: Graphical-statistical method for the study of structure and reaction processes of coal, *Fuel*
295 *Processing Technology*, 29, 269-228, 1950.
- 296 Vollmer, W., Blanot, D., and De Pedro, M. A.: Peptidoglycan structure and architecture, *FEMS Microbiology*
297 *Reviews*, 32, 149-167, <https://doi.org/10.1111/j.1574-6976.2007.00094.x>, 2008.
- 298 Vorobev, A., Sharma, S., Yu, M., Lee, J., Washington, B. J., Whitman, W. B., Ballantyne, F. t., Medeiros, P. M.,
299 and Moran, M. A.: Identifying labile DOM components in a coastal ocean through depleted bacterial
300 transcripts and chemical signals, *Environmental Microbiology*, 20, 3012-3030,
301 <https://doi.org/10.1111/1462-2920.14344>, 2018.
- 302 Waggoner, D. C., Chen, H., Willoughby, A. S., and Hatcher, P. G.: Formation of black carbon-like and alicyclic
303 aliphatic compounds by hydroxyl radical initiated degradation of lignin, *Organic Geochemistry*, 82, 69-
304 76, <https://doi.org/10.1016/j.orggeochem.2015.02.007>, 2015.
- 305 Waggoner, D. C., and Hatcher, P. G.: Hydroxyl radical alteration of HPLC fractionated lignin: Formation of new
306 compounds from terrestrial organic matter, *Organic Geochemistry*, 113, 315-325,
307 <https://doi.org/10.1016/j.orggeochem.2017.07.011>, 2017.
- 308 Waggoner, D. C., Wozniak, A. S., Cory, R. M., and Hatcher, P. G.: The role of reactive oxygen species in the
309 degradation of lignin derived dissolved organic matter, *Geochimica et Cosmochimica Acta*, 208, 171-184,
310 <https://doi.org/10.1016/j.gca.2017.03.036>, 2017.
- 311 Wagner, S., and Jaffé, R.: Effect of photodegradation on molecular size distribution and quality of dissolved black
312 carbon, *Organic Geochemistry*, 86, 1-4, <https://doi.org/10.1016/j.orggeochem.2015.05.005>, 2015.
- 313 Wagner, S., Ding, Y., and Jaffé, R.: A new perspective on the apparent solubility of dissolved black carbon,
314 *Frontiers in Earth Science*, 5, 1-16, <https://doi.org/10.3389/feart.2017.00075>, 2017.
- 315 Wagner, S., Jaffé, R., and Stubbins, A.: Dissolved black carbon in aquatic ecosystems, *Limnology and*
316 *Oceanography Letters*, 3, 168-185, <https://doi.org/10.1002/lo.10076>, 2018.
- 317 Wagner, S., Brandes, J., Spencer, R. G. M., Ma, K., Rosengard, S. Z., Moura, J. M. S., and Stubbins, A.: Isotopic
318 composition of oceanic dissolved black carbon reveals non-riverine source, *Nature Communications*, 10,
319 1-8, <https://doi.org/10.1038/s41467-019-13111-7>, 2019.
- 320 Wang, H., Zhou, H., Ma, J., Nie, J., Yan, S., and Song, W.: Triplet photochemistry of dissolved black carbon and
321 its effects on the photochemical formation of reactive oxygen species, *Environmental Science &*
322 *Technology*, 54, 4903-4911, <https://doi.org/10.1021/acs.est.0c00061>, 2020.
- 323 Wang, X., Xu, C., Druffel, E. M., Xue, Y., and Qi, Y.: Two black carbon pools transported by the Changjiang
324 and Huanghe Rivers in China, *Global Biogeochemical Cycles*, 30, 1778-1790,
325 <https://doi.org/10.1002/2016GB005509>, 2016.

- 326 Ward, C. P., Sleighter, R. L., Hatcher, P. G., and Cory, R. M.: Insights into the complete and partial
327 photooxidation of black carbon in surface waters, *Environmental Science: Processes & Impacts*, 16, 721-
328 731, <https://doi.org/10.1039/C3EM00597F>, 2014.
- 329 Ward, N. D., Keil, R. G., Medeiros, P. M., Brito, D. C., Cunha, A. C., Dittmar, T., Yager, P. L., Krusche, A. V.,
330 and Richey, J. E.: Degradation of terrestrially derived macromolecules in the Amazon River, *Nature*
331 *Geoscience*, 6, 530-533, <https://doi.org/10.1038/ngeo1817>, 2013.
- 332 Watrous, J., Roach, P., Heath, B., Alexandrov, T., Laskin, J., and Dorrestein, P. C.: Metabolic profiling directly
333 from the Petri dish using nanospray desorption electrospray ionization imaging mass spectrometry,
334 *Analytical Chemistry*, 85, 10385-10391, <https://doi.org/10.1021/ac4023154>, 2013.
- 335 Weishaar, J. L., Aiken, G. R., Bergamaschi, B. A., Fram, M. S., Fujii, R., and Mopper, K.: Evaluation of specific
336 ultraviolet absorbance as an indicator of the chemical composition and reactivity of dissolved organic
337 carbon, *Environmental Science & Technology*, 37, 4702-4708, <https://doi.org/10.1021/es030360x>, 2003.
- 338 Wetzel, R. G., Hatcher, P. G., and Bianchi, T. S.: Natural photolysis by ultraviolet irradiance of recalcitrant
339 dissolved organic matter to simple substrates for rapid bacterial metabolism, *Limnology and*
340 *Oceanography*, 40, 1369-1380, <https://doi.org/10.4319/lo.1995.40.8.1369>, 1995.
- 341 Wienhausen, G., Noriega-Ortega, B. E., Niggemann, J., Dittmar, T., and Simon, M.: The exometabolome of two
342 model strains of the *Roseobacter* group: A marketplace of microbial metabolites, *Front Microbiol*, 8, 1-
343 15, <https://doi.org/10.3389/fmicb.2017.01985>, 2017.
- 344 Wozniak, A., Bauer, J., Sleighter, R., Dickhut, R., and Hatcher, P.: Technical note: Molecular characterization of
345 aerosol-derived water soluble organic carbon using ultrahigh resolution electrospray ionization Fourier
346 transform ion cyclotron resonance mass spectrometry, *Atmospheric Chemistry and Physics*, 8, 5099-5111,
347 <https://doi.org/10.5194/acp-8-5099-2008>, 2008.
- 348 Wozniak, A. S., Goranov, A. I., Mitra, S., Bostick, K. W., Zimmerman, A. R., Schlesinger, D. R., Myneni, S.,
349 and Hatcher, P. G.: Molecular heterogeneity in pyrogenic dissolved organic matter from a thermal series
350 of oak and grass chars, *Organic Geochemistry*, 148, 1-18,
351 <https://doi.org/10.1016/j.orggeochem.2020.104065>, 2020.
- 352 Wünsch, U. J., Bro, R., Stedmon, C. A., Wenig, P., and Murphy, K. R.: Emerging patterns in the global
353 distribution of dissolved organic matter fluorescence, *Analytical Methods*, 11, 888-893,
354 <https://doi.org/10.1039/C8AY02422G>, 2019.
- 355 Xiao, Y., Carena, L., Näsi, M.-T., and Vähätalo, A. V.: Superoxide-driven autocatalytic dark production of
356 hydroxyl radicals in the presence of complexes of natural dissolved organic matter and iron, *Water*
357 *Research*, 1-8, <https://doi.org/10.1016/j.watres.2020.115782>, 2020.
- 358 Yavitt, J. B., and Fahey, T. J.: An experimental analysis of solution chemistry in a lodgepole pine forest floor,
359 *Oikos*, 43, 222-234, <https://doi.org/10.2307/3544772>, 1984.
- 360 Zeng, Y., Hong, P. K. A., and Wavrek, D. A.: Chemical-biological treatment of pyrene, *Water Research*, 34,
361 1157-1172, [https://doi.org/10.1016/S0043-1354\(99\)00270-5](https://doi.org/10.1016/S0043-1354(99)00270-5), 2000a.
- 362 Zeng, Y., Hong, P. K. A., and Wavrek, D. A.: Integrated chemical-biological treatment of benzo[a]pyrene,
363 *Environmental Science & Technology*, 34, 854-862, <https://doi.org/10.1021/es990817w>, 2000b.
- 364 Zimmerman, A. R.: Abiotic and microbial oxidation of laboratory-produced black carbon (biochar),
365 *Environmental Science & Technology*, 44, 1295-1301, <https://doi.org/10.1021/es903140c>, 2010.
- 366 Zimmerman, A. R., Gao, B., and Ahn, M.-Y.: Positive and negative carbon mineralization priming effects among
367 a variety of biochar-amended soils, *Soil Biology & Biochemistry*, 43, 1169-1179,
368 <https://doi.org/10.1016/j.soilbio.2011.02.005>, 2011.